

## Response to reviewers' comments

We would like to thank the reviewers for their helpful comments. These are repeated below (in italics) followed by our responses.

### Reviewer 1

*My main demands are (see specific comments) - to rewrite sections 3.2 and 3.3 clearly presenting and separating results & analysis of o mean emission and sinks versus their changes, o results & analysis global scale versus regional o results & analysis of emissions versus the sinks - to comment on all emissions (anthropogenic microbial emission poorly commented) - to report emission changes in Tg/yr between 2 time periods and not in trends (Tg/yr<sup>2</sup>), - to add a table with emissions changes, - to add a discussion section where comparison with other studies can be grouped.*

We agree that both section 3.2 and 3.3 could be made clearer by providing more details and separating the results as follows:

- Prior and posterior comparison.
- Posterior trends both globally and regionally.
- Source and sink attribution from inversion.
- Integrate sensitivity.

We agree that the reviewer suggestions will improve the manuscript significantly and thank him/her for them. We have addressed the following specific comments relating to the general remarks above.

*P2 L15-20: Please note that these mean isotopic signatures are associated with rather large range. It may be worth writing also that total source signature is -51/-53‰.*

We have included the total source signature as suggested and highlight the categories given are in a broad range.

*P2 L25: "although they emphasised that the problem is not very well constrained by existing data I suggest to be more precise: although these two studies cannot discard the hypothesis that OH is not changing.*

We agree that the discussion of the conclusions drawn by Rigby et al., 2017 and Turner et al., 2017 was not detailed enough and as a result we have now also commented that their results could not discard the hypothesis of no OH change.

*P3 L5: please define shortly here "synthesis inversion" (3D modelling, reduction of the size of flux and observation spaces to solve the inverse problem, ...) focusing on the improvement compared to box models.*

We agree that giving a short sentence describing the synthesis inversion and comparing it to box models would be useful here. This has been included.

*P3 L18: what is a one-year inversion spin-up? please detail a bit.*

We have appended the sentence to explain the one year spin-up is used to optimise the model CH<sub>4</sub> and δ<sup>13</sup>CH<sub>4</sub> concentration fields relative to the observations.

*P3 L21-22: what is the influence of this choice? what do you take for geological emissions ? It might be worth making a sensitivity test by taking the values from Saunois et al (2016) (update of the Kirschke paper, please quote) instead of the Schwietzke paper.*

We agree that the relevance to the Kirschke study is outdated and we have updated the reference to the more recent Saunois et al. study. The decision to scale to Schwietzke et al. estimates was based

on their development of isotope source signatures, which we felt was relevant for this paper. However, we agree that the Sauniois et al. study provides more thorough estimates, and a sensitivity study using both estimates would be interesting, a comparison of the budgets between the two studies is however beyond the scope of this work.

*P3 L26: I would be worth mentioning which of your sources is prescribed in the prior with interannual variability. Maybe in Table 1.*

OK. We have updated Table 1 to include which source/sinks vary interannually.

*P3 L30: I understand that you compute monthly response functions using the forward model? Please specify this here.*

Yes. We have updated the text to specify the monthly emissions can be used to assess variability.

*P4 L5: Why increasing OH and CI? Please justify this choice?*

By adjusting the OH, the sensitivity can be diagnosed, and this sensitivity remains the same whether fields are increased or decreased. A small feedback is present in the model setup due to CH<sub>4</sub> loss rate being dependent on CH<sub>4</sub> concentration. To reduce the impact of this, the sensitivity simulations only adjust the OH concentrations by a small amount (1%). This has been added to the text.

*P4 L9-10 and P5 L9-14: Not clear. How do you deal with the long-term equilibration of 13CH4 (e.g. Tans 97 paper) with 1-yr inversions?*

The inversions are performed for monthly emissions, although the total inversion length (13 years) comprises a series of the 1-year inversions mentioned. We have included that the 1-year inversions are performed for computational reasons, and by rerunning the forward model with posterior fluxes we are able to provide initialisation fields for the subsequent year. In effect, this serves as a single 13-year inversion for the purpose of long-term equilibration, because the previous year posterior fluxes influence future concentration fields. The posterior fluxes are not influenced by observations beyond the 1 month window; however the timescale of changes in the isotopic signature are still captured by the inversion.

Our results suggest that given the source signature change in the total posterior emissions from 2007, the response time of atmospheric  $\delta^{13}\text{CH}_4$  is comparable to that of CH<sub>4</sub> at the spatial scales resolved in this study. This suggests the long-term equilibration of  $\delta^{13}\text{CH}_4$  shown by Tans (1997) using a box model approach is not applicable to the 3D CTM used here.

*P4: I understand that isotopic signature are not optimized in this procedure. Please precise this point.*

We agree that more details were needed. In the submitted paper there was a comment P12 L30 that mentions this, but we have added a new sentence on P4 to highlight this point.

*P5 L4-7: Bousquet et al 2011 addressed this point and tested a second iteration with only small impact on the inversion results, so consistent with your hypothesis. It might be worth quoting.*

We thank the reviewer for pointing this out and have updated the text to include the finding of Bousquet et al. (2011).

*P5 L9: "The model OH is constrained by CH4 and  $\delta^{13}\text{CH}_4$ ": this is a weak constraint as many combination of total source and mean OH can fit the atmospheric changes. Please notice it here? With such a configuration you largely depend on the prior for the mean emissions and sinks so I would not insist a lot in the paper on the posterior versus prior comparison but more on budget changes with time and between your different inversions.*

We agree that multiple plausible emission/sink scenarios could exist to fit the observations, we highlight that a paucity of observations prevent a single solution. However, the 3D model approach,

over the box-model approach reduces the combination spread. We have updated the results and summary to remove the focus on prior v posterior and focus more on budget changes as suggested (Tables 4, 5 and 6).

*P6 L10-11: Putting only one value of uncertainty for all stations is a bit crude as model error will not be the same for remote sites of the southern hemisphere and continental sites of the northern hemisphere. More refinement is needed here or at least a sensitivity test varying observational errors.*

We agree that the magnitude of the model transport error will differ between sites, however the quantification of this transport error is beyond the scope of this work. We have added text outlining that the assumption is made as an estimate and not quantitatively derived.

*P6: It might worth doing a sensitivity test with more atmospheric observations, when appearing in the network. The apparition of stations is an issue but can help analysing regional gradients more safely. As you perform yearly inversions, why not adding each year the stations appearing in your inversions?*

We agree both approaches could be adopted. If we included additional sites as and when they became available, then we would gain more information from the inversion. We did not adopt this approach for the same reason as we did not use GOSAT retrievals in the inversion, intermittently adding observations would influence trend results and could result in disjointed posterior estimates, which result from the inclusion of new observations. Therefore, for long-term trend detection we opted not to append the observation set. For more accurate instantaneous posterior estimates we agree new observations should have been used, but as the key aim of the paper was to investigate the trend before and after 2007 we chose to omit new observations.

*P7 L22: "slow inter-hemispheric transport within the model": please provide the Inter Hemispheric Time and/or a reference for this possibly from Transcom experiments?*

We have added text referring to the Patra et al. (2011) Transcom study with reference to the Inter Hemispheric transport.

*P7 L27: For Garmisch did you try to extract the station at different level in your model?*

The averaging kernel is applied from the nearest model pressure level to the TCCON surface pressure and upwards, which is done to remove lower levels from the model output. It is possible that sub-grid scale variations in concentration due to orography, which are not accounted for due to smoothing in the coarse resolution model, is a cause of the model bias. We have not attempted to extract station information at different model levels due to the complex gradients related to orography and vertical profiles.

*P7 L29: 21.4 ppb is still a quite large value. Can you at least make hypotheses to explain them?*

We agree these are still relatively large errors, although they are more than halved relative to the prior and are approximately 1% of the concentration. A possible reason for this is that only surface observations are used in the inversion and not column information measured by TCCON. We have added text outlining this limitation.

*P8 – sect3.2: "OH concentrations in INV-FULL and INV-CH4 are relatively constant throughout the period 2007-2015 (Figure 5) but these values are smaller by  $1.8\pm0.4\%$  and  $0.3\pm0.5\%$ " : unclear : do OH is constant or diminishing. Please clarify. Also, I find a bit strange to start by the section by the sink and not by source changes.*

We agree it was somewhat unclear and have restructured the sentence to clarify that OH concentrations between 2007 and 2015 are constant but are lower relative to the previous years (2003-2006). In regard to structuring, the section has now been reformulated following the suggestions within this comment and the following comments.

*P8 L9-10: It may be good to refer to the sensitivity test on OH (S9) here.*

We agree the original structure could be difficult to follow. We have now referenced the sensitivity section here for completeness.

*P8 L11-15: Mixing the mean changes compared to the prior and the time changes from 2003-2006 to post-2007 period is confusing. What about change in agriculture flux? I suggest to group discussions on the mean sources and sinks global and regional (table 4) and then address the changes (table 5).*

We have rewritten this section to clearly separate out mean attribution and trends in sources and sinks.

*P8 L24: How did you estimate the 30% for OH and 60%/10% values? Did you use S9? Please justify.*

We agree this was not made clear in the results, and we have updated the text to explain. The inversion results were used in a simple box model to attribute contributions of each source and sink to the observed CH<sub>4</sub> trend. The details of the box model are found in McNorton et al (2016b).

*P8: The choice to report changes in trends (Tg yr<sup>-2</sup>) is a bit technical. A suggestion would be to report emission change between two periods (e.g. 2003-2005 and 2012-2015) in Tg/yr and quantify the % of contributions from this.*

We agree that reporting the results as the shift between the two periods is clearer. As the reviewer mentioned the structure of the section did not flow and this was one of the reasons. As a result, we have restructured the section to bring these two sets of analysis into the same part. We have kept the more technical growth rates (Tg yr<sup>-2</sup>), as they provide information about the rate of change, but have also now included Tg/yr and the % contribution.

*Table 5: There are some values worth to comment in your analysis: increase emissions from NA? dipole +0.59 / -0.58 for energy between NA and EA? wetland increase in Eurasia? Why? visible in other studies?*

The inversion ability to constrain NA and EA energy sector emissions independently reveals potential issues as discussed in Section 3.2. As a result, we have added in two sentence to describe a potential limitation in the model inversion system when used to distinguish between NA and EA energy sector emissions. The spatial distribution in wetland trends from previous studies remains uncertain and as a result is not used to inform the results of this study.

*Section 3.2: You do not comment waste sector (+0.46 in your table 5). Indeed, anthropogenic microbial emission contribute almost as much as wetlands (0.46 and 0.2 trends globally versus 0.8 for wetlands). Please add comments on anthropogenic microbial emission changes.*

We agree that whilst the magnitude of the waste emission changes is not as large as either energy sector or wetland changes, the relative change is larger and therefore should be commented on. We have now included this in our results.

*P9 L5-9: You have very few stations constraining NA inland emissions. It should be notices here as the increased inferred emissions over NA is a hot topic. Again including NA inland stations in a sensitivity inversion seems necessary to confirm such a result. In any case this has to be commented here.*

We agree the sparse observations over NA and EA may be the cause of some of these anomalous results, we have added this in as a caveat to the results.

*P10: It is a bit difficult to follow all the trends provided and to compare them to the standard inversion. I suggest to make a table with results of sensitivity test for global scale compared to INV-FULL (in Tg/yr difference between 2 periods and not trends in Tg/yr<sup>2</sup>). Then you can more clearly comment on the differences in the main text.*

We agree and have added this table in as Table 8, the results discussion now reflects what is shown in the table for clarity.

*P10 L7: “the magnitude in post-2006 changes is typically increased in S9”, please add something like: which is normal considering that constant OH as compared to decreasing OH in INV-FULL requires more emission change to match atmospheric observations.*

We agree that this point should be made clear, i.e. that the results are expected due to the removal of the OH sensitivity. We have added a line explaining this.

*P10 L21-22: Again, please acknowledge here that global total OH versus total emissions are not very well constrained without an external proxy as many combination can match the growth rate. You largely rely to the prior in this case so I would not insist a lot on the posterior versus prior comparison but more on budget changes with time and between your different inversions.*

We agree that the paper needed to focus more on the trend/shift over the period and less on the comparison with the prior. We have added a comment here and elsewhere in the paper to emphasise this point.

*P11 L15-30: This comparison with EDGAR should be in a discussion section between 3.3 and conclusions where you could compare your results with other studies. More references to previous results would be good e.g. Pouter et al. 2017 for wetlands, Saunio et al., 2017 ACP for all sources, more precise comparison about OH with Rigby and Turner papers.*

We agree that the ordering of discussion is confusing and have changed it as suggested. We have included reference to Saunio et al., (2017). Poulter et al. is not included because it only covers a subset of the period studied. We have also given quantitative comparisons to the Rigby and Turner papers.

*P11 L21-22: “As a result emissions from these regions are influenced by posterior emission changes and assumed to be underestimated in both magnitude and growth rate in the prior” : unclear to me, please rephrase.*

We agree this sentence is not clear. We have modified it to describe that the inversion system can attribute fluxes and trends at a regional level, but cannot diagnose spatial patterns at a sub-regional scale (for example national).

*P11 L27: I do not see this -2.2 Tg/yr<sup>2</sup> in Table 5? Please clarify.*

We agree this was not clear. We have clarified that the EDGAR comparison is for 2003-2012, when EDGAR data are available, while the figure in Table 5 (-0.58 Tg/yr<sup>2</sup>) is for 2003-2015. The EA energy sector emissions appeared to rebound slightly in later years.

*P12 L11: You do not believe your results? This sentence introduce confusion. Please rephrase it or remove it.*

OK. We have modified the sentence to state that whilst our findings provide the most likely explanation for the cause of the renewed growth, an alternative scenario could exist whereby OH remains unchanged; however, this is considered less likely.

*P12 L13: Saunio paper is not an inventory by a synthesis of inventories and inversions. Please rephrase.*

We agree we did not describe the Saunio paper correctly. We have modified this to explain the combination of inventories and top-down studies.

*P12 L27: Limitation of synthesis inversions (monthly means, coarse regions...) should also be mentioned here.*

We agree this is a caveat to the study and have added this in.

*P12 L31: What about NO<sub>2</sub> decrease in Asia in the late 2000s? Please mention this hypothesis as well.*

We have included a reference to the decreased NO<sub>2</sub> growth rate in the late 2000s, which approximately coincides with the renewed CH<sub>4</sub> growth.

## **Reviewer 2**

*What is the rationale for the regional division applied in the transport model and the inversion? Especially the large EA and AO emission regions combining countries and regions with very different socio-economic developments in the last decades are very questionable choices. As the inversion is set up right now it can, for example, not distinguish between Western Europe with well-established and generally decreasing CH<sub>4</sub> emissions from most sectors from emissions in Russia or North-East Asia. These are areas with potentially growing emissions from different sectors in the last decades. Although, these trends may be presented in the a priori it seems more likely that there are uncorrelated uncertainties in the emission estimates for these areas. Similar arguments can be found for a required sub-division between south-east Asia and Australia. In the end, the current sub-division alters the derived regional trends in the a posteriori emission very questionable. For example, opposing regional errors in the a priori trends in these large regions may alter it impossible for the inversion to correctly correct these trends. Instead the missing/excessive emissions may be laid down in/removed from regions for which little direct constraint is available from the utilised set of observations, but only a more global sensitivity exists in the model (such as the AM region). Maybe not surprisingly these are the regions for which the authors find the strongest changes in a posteriori emissions, a result that somewhat differs from conclusions in previous work. The regional sub-division certainly needs some further justification. This could be done by a more in-depth validation of the model performance at surface sites in contrasting areas like Europe vs. East Asia. For this the use of additional surface observations should be considered (see major comment 3).*

We agree that the coarse spatial grouping limits the validity of affects the results to an extent, although it provides more comprehensive information than a similar box model approach. Unfortunately, this approach does assume correlation over large geographical regions that span differing socio-economic regimes. However, aggregation errors such as these are a known drawback of the methodology used in our work, and we discuss this in the main text. To reduce computational cost 5 regions were chosen, although we agree future studies using a similar approach could potentially seek to increase, or vary geographically, the number of regions chosen. The regions were chosen based on socio-economic background but also natural emission regions, and were partially derived by grouping regions of the existing Transcom basis function map (DeFries *et al.*, 1994). Increasing the number of regions used in the inversion would also likely reduce the constraint provided by the limited number of observations used in the study (see next response for more details), which we tried to avoid.

We have now included this caveat in the conclusion and detailed that posterior emissions within a domain are incorrectly assumed to have perfect correlation. We have included that this likely results in a positive bias within a domain being offset by a negative bias elsewhere in the domain. We have referenced our justification for the chosen regions in section 2, with reference to DeFries *et al.* (1994).

*As stated correctly on page 2 line 23, Rigby *et al.* (2017) and Turner *et al.* (2017) both conclude that the problem of the post 2007 methane rise may be under-constrained using the observed CH<sub>4</sub> concentrations, 13CH<sub>4</sub>/12CH<sub>4</sub> ratios and other tracers. Their conclusion is based on simpler box-model simulations without detailed regional division of CH<sub>4</sub> emissions. In the present study an even larger number of unknowns is optimised through the inversion. Wouldn't this mean that the individual elements of the state vector are even less well constraint? The authors should spend some time*

*justifying why their more detailed results should be better constrained than those from box-model analyses. In this context it may be worth looking at the covariances in the a posteriori emission and OH factor as well. Large negative covariances may indicate that the inversion cannot clearly distinguish between regions and sectors.*

As touched on in the previous response, the number of emission regions and sectors in this study were chosen in order to try to maintain a balance between learning as much as possible about the geographical distribution of the source/sink trends, whilst not under-constraining the posterior solution through use of too large a state vector. In the event, we generally match the number of observations and the number of elements in the state vector quite closely. Our study uses a larger number of regions and observations than previous “box model” studies, along with realistic atmospheric transport representation, and as such provides extra information concerning the distribution of source/sink changes. However, as indicated by our posterior errors and similarly to the other studies mentioned here, the uncertainty of our results is still relatively high, particularly for the OH sink term, and we discuss this in our conclusions.

To investigate this further we have now included some example error posterior correlations, new Figure 11, showing that the error correlations of the off-diagonals is relatively small and therefore, the results are well constrained.

*The authors base their inverse flux estimates on a limited set of surface observations (22 flask sampling sites). This may be justified in order to keep the influence of CH<sub>4</sub> concentrations to 13CH<sub>4</sub>/12CH<sub>4</sub> ratios similar, with the latter only being available at this limited number of locations. However, for validation purposes there would be many more CH<sub>4</sub> observations available worldwide (flask and continuous). These should be evaluated as independent observations as well and may better than GOSAT and TCON observations demonstrate the success of the inverse flux estimate.*

We agree that the inclusion of surface site observations for independent validation would improve the evaluation. We have added two independent site validations (new figure 5) for both CH<sub>4</sub> and  $\delta^{13}\text{CH}_4$ . As mentioned, the  $\delta^{13}\text{CH}_4$  observations are somewhat limited by the duration of the time series and this has been noted in the updated text.

*P2L26f: Although the global a priori emissions by source category are available in Table 1 and regionally divided a posteriori emissions are given in Table 4, I am missing the same kind of information for the a priori. An additional table in the style of Table 4 but for the a priori emissions should be added.*

We agree that extra detail on the prior can be added for completeness and have now added this to table 4 and updated the text to include this.

*P4L7ff: If I correctly understand the inversion setup, the inversion step is performed on batches of 12 months. Does this mean that the emissions from the previous year are not influenced by the observations of the next year at all? Meaning that January observations will not influence December emissions from the previous year? This would result in December, but probably also November and October, emissions always being constraint by less observations than emissions in other months and, therefore, probably are less corrected from their a priori values and/or show systematically larger a posteriori uncertainties than emissions in other months. Was this observed in the a posteriori factors?*

We agree that the nature of the experimental setup results in early year emissions being constrained by more observations than those later in the year. This has been investigated and the posterior error is found to be similar in the early months to the later months. As a result, we do not think the influence of few observations constraining posterior emissions later in the year is noticeable. We have added this to the text and explained that the posterior error for January emissions is similar in magnitude to the error for December emissions.

*P5L16: The wording is not very precise here. J is a cost function and the inversion will find its minimum. J is not a minimisation function. Instead equation 4 represents the analytical minimum of equation 3.*

We agree that the wording is not clear here and have updated the text before equation 3 to indicate that we calculate the cost function to quantify the optimisation and before equation 4 the text now indicates that the minimum is found using the Tarantola and Valette equation.

*P5L24: R is not the covariance matrix of the observations alone. R contains the observation/model mismatch covariance. Later this fact is taken care of by adding a model uncertainty to R, but it should be correctly introduced here.*

We agree and have added in that R includes both observation and model error.

*P6L6: Was any month-to-month variability of the emissions included in the a priori? If yes where was it taken from?*

We did not include details of this in the original text, but have now corrected the text in page 3 line 25 to comment that prior emissions vary at a monthly timescale.

*P6L10f: This is a bit simplistic since the model uncertainty most likely varies with the location of the observation and the question how representative the model grid cell can be for a given site. There have been many different approaches in the past on how to assign site-dependent model uncertainties and, hence, this point should be justified a bit more.*

As noted by reviewer 1 this detail was not included in the original submission, we have included a sentence acknowledging that the magnitude of transport uncertainty varies between sites but due to a lack of information we have taken the simple approach and assumed all uncertainties are equal.

*P7L6 and elsewhere: A lot of this RMSE is due to a bias in the a priori simulation. It would be better to calculate a bias-corrected RMSE instead. The bias could be mentioned separately. In general it would be nice to include all these comparison statistics in a table as well (in the main text for all discussed inversions and observational data sets and in the supplementary material for all sensitivity inversions).*

We agree that the high RMSE values are caused by the bias between the prior and observations. We have now included an explanation of this cause in elevated RMSE. We have also referenced it to Figures 1 to 4, showing the bias against both assimilated and non-assimilated observations. We have used RMSE and not bias-corrected RMSE because the bias is not constant and grows from zero at the start of the simulation. As a result the total offset contributes to the overall error and is reported.

*P7L23f: I don't think it is the model that is growing here. What about 'simulated atmospheric methane growth rates' instead?*

We agree the wording is much clearer as suggested and have made the recommended changes.

*P7L27f: This behaviour is very strange. For all other sites an increase in concentrations from a priori to a posteriori simulations was observed. Why not for Garmisch, a central European site not too far away from the Bremen site, where differences in the a priori and a posteriori simulations are as expected? One potential source of mismatch may be the location of Garmisch at the northern edge of the Alps, potentially introducing large mismatches due to smoothed model topography. Still this would not explain the lack of an increase from a priori to a posteriori. Although a detail, this needs to be checked again.*

We agree this mismatch is unusual and have since checked the data. We have spotted a coding error that led to this result and have now fixed it to present the actual posterior estimates and have updated the text and plots accordingly.

*P8L5 and Figure 5: The estimated a posteriori OH time series should also be compared with work by other authors (e.g. Rigby et al. 2017). If OH is really the main driver of the post 2007 CH<sub>4</sub> rise it would be good to know how TOMCAT OH compares to previous work.*

We agree that more detailed comparison with other work should be made. We have re-written section 3 and included detailed comparison with both the Rigby et al. and Turner et al. studies.

*P8L15: A reference to Table 6 should be added here.*

This section has been rewritten, but we have now referenced Table 6 in the equivalent section of the re-written version.

*P9L11: A reference to Figure 5 should be added here.*

This section has been rewritten, but we have now referenced Figure 5 (now 6) in the equivalent section of the re-written version.

*P9L28f: How similar? These numbers are not given anywhere. One can only guess them from the figures. A table (like Table 4) with the a posteriori emissions for the INVCL case should be provided and the same for all sensitivity inversion (supplement).*

We agree a quantitative description of the posterior estimates from the different sensitivities is important, as a result we have included Table 8, which provide these values.

*P9L28f: How is the a posteriori performance for this experiment (S4)? Just because one sensitivity run gives different a posteriori emissions it doesn't have to be wrong. But if it also fails to reproduce the observations, then the given conclusion may be correct.*

We agree that any single sensitivity test might provide a more realistic representation and therefore should not be discounted just because it is an outlier. Most of the sensitivities provide similar performance when compared with observations; with some exceptions. For S4 we isolate it as an anomaly due to the magnitude of the interannual variability, we consider annual energy sector variability for S4 to be too large to represent a realistic scenario. For example, in 2009 global energy sector emissions are around 3 times higher than the values for other years. We have added in this justification for our conclusion in the text.

*P10L31f: This sounds a bit like the authors of Rigby et al. worked on the current study as well. Which is not the case. This work may extend the previous work by using a more complex transport model, but other than that the approaches are fairly different and unrelated (inversion system, used observations, etc.). So I would not write that it extends the work of Rigby or others, but rather it adds to the results gained by others.*

We agree the wording is ambiguous and have clarified the text to now indicate that we added to the results from other studies.

*P11L7: 'larger errors'. What kind of errors? Needs to be repeated here.*

We agree this is also ambiguous, we have commented on the inversion being under constrained and the correlation with observations being reduced.

*P11L7f: The sentence 'The constraint improves when the  $\delta^{13}\text{CH}_4$  observations are introduced' should be re-written to be more precise. What about: 'The agreement of the simulations with observations improved when additional  $\delta^{13}\text{CH}_4$  observations are used to constrain CH<sub>4</sub> fluxes.'*

We agree the current structure does not explain the improvement, we have modified the text following the suggested re-write.

*P11L12: This conclusion is just based on the different trend compared with GOSAT, whereas the trend in surface observations was captured well in the a posteriori simulation. Does that mean that there is a potential trend in the bias between GOSAT and surface observations? Would there be any GOSAT validation studies that may provide some clarification?*

We have now extended the validation to apply not only to GOSAT, but also TCCON. This has been added to the results and conclusion, both in the text and figures. From this the posterior underestimates the growth in both GOSAT and TCCON, suggesting that there is no measurement bias in GOSAT. The reason for the bias between surface and column measurements is certainly interesting and might highlight column errors in the posterior, although potential bias in column observations might play a role. We have included this in the conclusion.

*P11L15f: Once again: There are more surface observations available than used in this study. They should be used for validation during this critical period.*

We have now included independent surface observations for validation.

*P11L29: It is unclear which period is referred to here? Table 5 suggests a growth rate in the energy sector of the AO region of 1.5 Tg yr<sup>-2</sup> the text states -2.2 Tg yr<sup>-2</sup>. What is correct?*

The text has now been updated, the text and table provide different values based on different time periods, 2003-2015 and 2003-2012.

*P12, 1st paragraph: This section should also repeat what was stated in the introduction concerning previous inverse modelling studies (P2L21ff), especially since the presented results contradict/correct these earlier findings.*

This discussion has now moved to the results section and details the comparison with existing studies in more depth to reflect what was in the introduction.

*Figure1: It is impossible to see the red dotted lines in many of the sub-panels (also the ones for  $\delta^{13}\text{CH}_4$ ). Either the figure needs to be enlarged/split or an additional color and solid line should be used for INV-CH<sub>4</sub>.*

We agree, and the plot has been updated with a new colour for the CH<sub>4</sub>-only inversion.

*Table1, Table4, Table6: These should also contain the uncertainty estimates.*

We agree that error values for table 1 and table 4 provide clear information on posterior uncertainties, for table 6 we have included the uncertainties more in the text and figures for clarity as the tables already contain a lot of information.

*Table1: Maybe I missed this before, but does the missing number for the soil sink mean that it was neglected completely? If it was only not-optimised its value should still be part of this table.*

We agree the model soil sink value should be given, we have added it to the table for the prior value; although because it is not optimised in the inversion we do not provide a posterior value.

# Attribution of recent increases in atmospheric methane through 3-D inverse modelling

5 Joe McNorton<sup>1,2</sup>, Chris Wilson<sup>1,3</sup>, Manuel Gloor<sup>4</sup>, Rob Parker<sup>3,5</sup>, Hartmut Boesch<sup>3,5</sup>, Wuhu Feng<sup>1,6</sup>, Ryan Hossaini<sup>7</sup>, Martyn Chipperfield<sup>1,3</sup>

<sup>1</sup> School of Earth and Environment, University of Leeds, Leeds, UK.

<sup>2</sup> Research Department, European Centre for Medium-Range Weather Forecasts, Reading, UK.

<sup>3</sup> National Centre for Earth Observation, University of Leeds, Leeds, UK.

<sup>4</sup> School of Geography, University of Leeds, Leeds, UK.

10 <sup>5</sup> Earth Observation Science Group, Department of Physics and Astronomy, University of Leicester, Leicester, UK.

<sup>6</sup> National Centre for Atmospheric Science, University of Leeds, Leeds, UK.

<sup>7</sup> Lancaster Environment Centre, Lancaster University, Lancaster UK.

Correspondence to: Joe McNorton (Joe.McNorton@ecmwf.int)

## Abstract.

15 The atmospheric methane (CH<sub>4</sub>) growth rate has varied considerably in recent decades. Unexplained renewed growth after 2006 followed seven years of stagnation and coincided with an isotopic trend toward CH<sub>4</sub> more depleted in <sup>13</sup>C, suggesting changes in sources and/or sinks. Using surface observations of both CH<sub>4</sub> and the isotopologue ratio value (δ<sup>13</sup>CH<sub>4</sub>) to constrain a global ~~3D~~3-D chemical transport model (CTM), we have performed a synthesis inversion for source and sink attribution. Our method extends on previous studies by providing monthly and regional attribution of emissions from 6 different sectors and changes in atmospheric sinks for the extended 2003-2015 period. Regional evaluation of the model CH<sub>4</sub> tracer with independent column observations from the Greenhouse gases Observing SATellite (GOSAT) shows improved performance when using posterior fluxes (R = 0.94-0.96, RMSE = 8.3-16.5 ppb), relative to prior fluxes (R = 0.60-0.92, RMSE = 48.6-64.6 ppb). Further independent validation with data from the Total Carbon Column Observing Network (TCCON) shows a similar improvement in the posterior fluxes (R = ~~0.90~~0.87, RMSE = ~~18.8~~14.4 ppb) compared to the prior (R = ~~0.7~~0.69, RMSE = ~~55.3~~39 ppb). Based on these improved posterior fluxes, the inversion results suggest the most likely cause of the renewed methane growth is a post-200~~6~~6 1.8±0.4% decrease in mean OH, a 12.9±2.7% increase in energy sector emissions, mainly from Africa/Middle East and Southern Asia/Oceania, and a 2.6±1.8% increase in wetland emissions, mainly from Northern Eurasia. The posterior wetland increases are in general agreement with bottom-up estimates, but the energy sector growth is greater than estimated by bottom-up methods. The model results are consistent across a range of sensitivity analyses performed.

25

30 When forced to assume a constant (annually repeating) OH distribution, the inversion requires a greater increase in energy sector (13.6±2.7%) and wetland (3.6±1.8%) emissions ~~and but also introduces~~ an 11.5±3.8% decrease in biomass burning emissions. Assuming no prior trend in sources and sinks slightly reduces the posterior growth rate in energy sector and wetland emissions, and further increases the ~~ampl~~ampl magnitude of the negative OH trend. We find that possible tropospheric Cl variations do not to influence δ<sup>13</sup>CH<sub>4</sub> and CH<sub>4</sub> trends, although we suggest further work on Cl variability is required to fully diagnose

Formatted: Font: 10 pt

Formatted: Font: 10 pt

this contribution. While the study provides quantitative insight into possible emissions variations which may explain the observed trends, uncertainty in prior source and sink estimates and a paucity of  $\delta^{13}\text{CH}_4$  observations limit the ~~accuracy~~ robustness of the posterior estimates.

## 1 Introduction

5 The atmospheric concentration of methane ( $\text{CH}_4$ ) has been increasing globally since 2007, following a slowdown in growth from 1999 to 2006 (Dlugokencky *et al.*, 2017). The onset of the observed increase in  $\text{CH}_4$  coincides with an isotopic trend to lighter  $\text{CH}_4$ , more depleted in  $^{13}\text{C}$  (Nisbet *et al.*, 2014). The  $^{13}\text{CH}_4$ : $^{12}\text{CH}_4$  ratio (denoted by the  $\delta^{13}\text{CH}_4$  value) is controlled by both the isotopic signatures of the sources and the isotopic fractionation associated with atmospheric  $\text{CH}_4$  sinks. Broadly speaking, the emission types can be categorised into the relatively light biogenics ( $\sim$ -62‰), heavier fossil fuels ( $\sim$ -44‰) and  
10 the even heavier biomass burning emissions ( $\sim$ -22‰) (Schwietzke *et al.*, 2016, resulting in a total source signature of between -51‰ and -53‰. ~~(Schwietzke *et al.*, 2016).~~ Isotopic fractionation in the atmosphere by the reaction with the hydroxyl (OH) radical and chlorine (Cl) atoms enriches  $^{13}\text{CH}_4$ , causing a background atmospheric  $\delta^{13}\text{CH}_4$  of  $\sim$ -47‰.

Previous studies have used simple global box-models for source and sink attribution of recent atmospheric  $\text{CH}_4$  trends, with  
15 contradictory findings. Nisbet *et al.* (2014; 2016) and Schaefer *et al.* (2016) suggested that either increased wetland or agricultural emissions were the likely cause while Rigby *et al.* (2017) and Turner *et al.* (2017) found the most likely explanation to be a decreased global mean OH concentration. The latter two studies, although they emphasised that the problem is not very well constrained by existing data and as a result could not discard the hypothesis that OH is not changing. These approaches are able to isolate the three emission categories noted above, and sometimes sink terms. Specific attribution, for example  
20 between wetlands and agricultural emission changes, requires spatial representation of both  $\text{CH}_4$  and  $\delta^{13}\text{CH}_4$ . The box-model approach provides little or no information of spatial variation in posterior emission estimates, preventing regional attribution. Rice *et al.* (2016) performed a ~~3D3-D~~ chemical transport model (CTM) inversion using  $\text{CH}_4$  and isotopologue measurements over the period 1984 to 2009. They found a  $24 \text{ Tg yr}^{-1}$  increase in fugitive fossil fuel emissions between 1984 and 2009, most of which occurred after 2000. The trend in their inversion appeared similar to their prior emission estimates. Although they  
25 used a 3D3-D CTM is used in their study the posterior emissions were calculated globally and not regionally. Furthermore, their study did not focus on the possible role of OH variations and did not consider inversions after 2009, so only captured two years of the continued post-20076 growth.

Here we perform a synthesis inversion using the TOMCAT 3-D CTM, building on previous work (Bousquet *et al.*, 2006;  
30 Bousquet *et al.*, 2011; Rigby *et al.*, 2012; Schwietzke *et al.*, 2016; Rice *et al.*, 2016) and using surface measurements of both  $\text{CH}_4$  (Dlugokencky *et al.*, 2017) and  $\delta^{13}\text{CH}_4$  (White *et al.*, 2017). The synthesis inversion technique uses the forward 3-D CTM to optimise monthly  $\text{CH}_4$  emissions over relatively large regions and for multiple source sectors, this spatial inversion approach

is not present in existing box model inversions. We investigate regional source contributions and the roles of tropospheric OH and Cl in the recent growth of CH<sub>4</sub>. From this we derive possible source and sink changes between 2003 and 2015 which best fit the observations.

## 2 Models and Observations

### 5 2.1 Chemical Transport Model

#### 2.1.1 Forward model

The TOMCAT global CTM (Chipperfield *et al.*, 2006) has previously been widely used to simulate CH<sub>4</sub> trends and been evaluated against observations (e.g. Patra *et al.*, 2011; Wilson *et al.*, 2016; Parker *et al.*, 2018). Here we base CH<sub>4</sub> synthesis inversions on TOMCAT simulations at 2.8° × 2.8° resolution with 60 vertical levels from the surface to 60 km for 2003-2015.

10 The simulations used meteorological forcing data from the 6-hourly European Centre for Medium-Range Weather Forecasts ERA-Interim reanalyses (Dee *et al.*, 2011). The model was spun up from a 1977 initialisation field before the mean global CH<sub>4</sub> and δ<sup>13</sup>CH<sub>4</sub> were rescaled to match NOAA observations in January 2002. A one-year inversion spin-up was then performed for 2002, [to optimise the 3-D CH<sub>4</sub> and δ<sup>13</sup>CH<sub>4</sub> concentration fields relative to observations](#) and the results shown here begin in January 2003.

15

[Monthly varying methane emissions from McNorton \*et al.\* \(2016a\)](#) were updated using revisions based on Schwietzke *et al.* (2016), which increased fossil fuel emissions and decreased biogenic emissions compared to the estimates in [Saunois-Kirshcke \*et al.\* \(2016\)](#). OH and stratospheric CH<sub>4</sub> loss fields were taken from McNorton *et al.* (2016b) and a TOMCAT-derived tropospheric Cl loss field (Hossaini *et al.*, 2016) was applied for the first time in our model.

20

Emissions were grouped into individual tracers for agriculture (excluding rice), biomass burning, energy, rice, waste, wetlands and 'supplementary', made up of the remaining sources (geological, hydrates, oceans and termites). Each source type, excluding 'supplementary', was then sub-divided into five geographic regions; North America (NA), Northern Eurasia (EA), South America (SA), Africa and Middle East (AM), and South Asia and Oceania (AO) (see [Figure 6](#)[Figure 7](#)). [These regions](#)

25

[were chosen by grouping existing Transcom regions \(DeFries \*et al.\*, 1994\) and considering both socio-economic and biome similarities](#). To assess [monthly](#) emission variability ~~over time~~, individual tracers were simulated for each month of the year, excluding 'supplementary' emissions, which were simulated annually. Emissions were further split into separate <sup>12</sup>CH<sub>4</sub> and <sup>13</sup>CH<sub>4</sub> tracers using isotopic source signatures taken from Schwietzke *et al.*, (2016) (Table 1), resulting in 6 source types over 5 regions for 12 months and 2 isotopologues, with an additional 5 regions for 'supplementary' sources (a total of 730 tracers).

30

Kinetic fractionation (KF, Table 1) was accounted for in the atmospheric loss of <sup>13</sup>CH<sub>4</sub>. The simulated tracers were then used to calculate CH<sub>4</sub> concentration and δ<sup>13</sup>CH<sub>4</sub> values. To investigate sensitivity to OH and Cl variations, three additional

simulations were performed, a control, an OH-enhanced simulation (1% increase) and a tropospheric Cl-enhanced simulation (1% increase). Any feedback, on the CH<sub>4</sub> term within the loss rate, from the small adjustments made (1%) is assumed to be negligible.

### 2.1.2 Synthesis inversion

5 Our global synthesis inversions build on techniques used in Bousquet *et al.*, (2006), Bergamaschi *et al.*, (2007) and Rigby *et al.*, (2012). Prior estimates of sources and sinks, uncertainty estimates, and observations of both CH<sub>4</sub> and δ<sup>13</sup>CH<sub>4</sub> were used to quantify posterior estimates of sources and sinks. Posterior estimates were then used in a second forward simulation for the same year, which provided an initialisation field for the subsequent year. The inversion method is limited by the assumption that source signatures are known.

10

For the inversion including OH concentrations in the state vector we consider the total simulated CH<sub>4</sub> mixing ratio ( $\varphi$ ) and the δ<sup>13</sup>CH<sub>4</sub> value ( $\psi$ ) at time,  $t$ , at each measurement location,  $l$ . These are described as a linear combination of contributions from  $n_{reg}$  emission regions separated into  $n_{month}$  months and  $n_{source}$  emission sectors, loss due to OH, fractionation due to OH, the initial mixing ratio at the location,  $\varphi_{ini}$ , and the initial δ<sup>13</sup>CH<sub>4</sub> value at the location,  $\psi_{ini}$ :

15

$$\varphi(\mathbf{x}, l, t) = \sum_{s=1}^{n_{source}} \sum_{i=1}^{n_{reg}} \sum_{m=1}^{n_{month}} x_{i,m,s} \frac{\Delta\varphi\mathbf{x}}{\Delta x_{i,m,s}}(l, t) + x_{OH} \frac{\Delta\varphi\mathbf{x}}{\Delta x_{OH}}(l, t) + x_{ini} \varphi_{ini}(l) \quad (1)$$

$$\psi(\mathbf{x}, l, t) = \sum_{s=1}^{n_{source}} \sum_{i=1}^{n_{reg}} \sum_{m=1}^{n_{month}} x_{i,m,s} \frac{\Delta\psi}{\Delta x_{i,m,s}}(l, t) + x_{OH} \frac{\Delta\psi}{\Delta x_{OH}}(l, t) + \psi_{ini}(l) \quad (2)$$

20

Note that we use  $\Delta$  here to represent change, in order to avoid confusion with the isotopologue δ<sup>13</sup>CH<sub>4</sub>. Basis functions  $\frac{\Delta\varphi\mathbf{x}}{\Delta x_{i,m,s}}$  and  $\frac{\Delta\psi}{\Delta x_{i,m,s}}$  are sensitivities of atmospheric CH<sub>4</sub> and δ<sup>13</sup>CH<sub>4</sub> at a particular time and location to an emission of 1 Tg of CH<sub>4</sub> from a region  $i$  during a particular month  $m$ , for an emission sector  $s$ . Each  $x_{i,m,s}$  is a scaling factor applied to the contribution from each basis function, and is initially set equal to the prior value of the emission. Similarly,  $\frac{\Delta\varphi\mathbf{x}}{\Delta x_{OH}}$  and  $\frac{\Delta\psi}{\Delta x_{OH}}$  are the sensitivities of the mixing ratio and δ<sup>13</sup>CH<sub>4</sub> at a measurement location to a change in the global OH concentration, linearised around the prior, and  $x_{OH}$  is initially set to be the prior OH concentration.  $x_{ini}$  is a dimensionless scaling factor initially set to be 1. Although the emissions in each region and source type are split into <sup>12</sup>CH<sub>4</sub> and <sup>13</sup>CH<sub>4</sub>, the relative emissions of each isotopologue from each region for each source type are not included as separate basis functions. The ‘state vector’  $\mathbf{x}$  comprises of the individual emission scaling factors  $x_{i,m,s}$ , for all  $i$ ,  $m$  and  $s$ , along with  $x_{OH}$  and  $x_{ini}$ . Sensitivity experiments performed for tropospheric Cl follow the same formulation with Cl terms replacing OH terms.

25

Varying atmospheric CH<sub>4</sub> concentrations in the inversions should in principle results in a non-linear feedback on OH concentration. This feedback is not accounted for and does not influence the offline OH field used in our inversion. To resolve this, an online OH field could in principle be used with an iterative minimization of the cost function. However, ; however, Bousquet et al. (2011) found that the variation small variation in CH<sub>4</sub> concentration between the prior and posterior is relatively small and assumed to have had a negligible influence on OH concentration.

The model OH is constrained by CH<sub>4</sub> and δ<sup>13</sup>CH<sub>4</sub> and but not by other species, such as methyl-chloroform (MCF). MCF was excluded because of uncertainty in emissions and a diminishing concentration (<5 ppt), particularly during the later period of the study (Liang et al., 2017). Due to the large uncertainty relative to the observed MCF concentrations in this period, including the extra species within the inversion would not add any extra constraint on the global OH concentration.

Independent inversions (INV-FULL) were performed for each year from 2003 to 2015. Initial conditions for each year are provided by a forward simulation for the previous year driven by derived posterior emissions and loss rates, with 2003 initial conditions taken from a 2002 spin-up inversion. To quantify the optimisation of the flux terms in each region and the sink term, we calculate the cost function, J. To estimate the flux contributions from each region we apply a minimisation function, which calculates the cost function, J.

$$J(\mathbf{x}) = \frac{1}{2}(\mathbf{x} - \mathbf{x}^b)^T \cdot \mathbf{B}^{-1} \cdot (\mathbf{x} - \mathbf{x}^b) + \frac{1}{2}(\mathbf{y} - \mathbf{G} \cdot \mathbf{x})^T \cdot \mathbf{R}^{-1} \cdot (\mathbf{y} - \mathbf{G} \cdot \mathbf{x}) \quad (3)$$

The value of this ‘cost function’ is dependent on the value of the state vector  $\mathbf{x}$ . The vector  $\mathbf{y}$  contains the observations.  $\mathbf{x}^b$  is the *a priori* estimate of  $\mathbf{x}$ , and  $\mathbf{B}$  is the error covariance matrix containing the uncertainties placed on the prior estimates, and the covariances between these uncertainties.  $\mathbf{G}$  is the sensitivity matrix, which maps  $\mathbf{x}$  onto the observations, and contains an array made up of the basis functions,  $\frac{\Delta \chi}{\Delta x}$  and  $\frac{\Delta \psi}{\Delta x}$  used in Eq. (1) and (2).  $\mathbf{R}$  is the diagonal error covariance matrix for the observations and model error.

The minimum of the cost function, which indicates the optimal source/sink scaling, is found using The minimum of the cost function is found using (Tarantola and Valette, 1982):

$$\mathbf{x}^a = \mathbf{x}^b + [\mathbf{G}^T \cdot \mathbf{R}^{-1} \cdot \mathbf{G} + \mathbf{B}^{-1}]^{-1} \cdot \mathbf{G}^T \cdot \mathbf{R}^{-1} \cdot [\mathbf{y} - \mathbf{G} \cdot \mathbf{x}^b] \quad (4)$$

where  $\mathbf{x}^a$  is the optimised set of scaling factors which minimise the value of  $J$ .

The posterior error covariance matrix  $A$  is calculated from:

$$A = [G^T \cdot R^{-1} \cdot G + B^{-1}]^{-1} \quad (5)$$

5 The initial prior uncertainty of each source within each region was set to 50%, based on uncertainties given by Kirschke *et al.*, (2013). We assume that increased uncertainty in sources with large interannual variability is offset by those sources having top-down (biomass burning) or process based (wetlands) interannually varying emissions in our simulations. We assumed small variability in energy sector emissions so assigned a 1-month offset correlation of 0.5, we have not assigned correlations between regions or months in the other prior emissions due to a lack of information. Global annual OH and CI are assumed to have an uncertainty of 2%; for OH this is based on estimated interannual variability (Montzka *et al.*, 2011). The impact of varying these uncertainties was investigated. Observational uncertainties were set at 10 ppb for CH<sub>4</sub> and 0.1‰ for δ<sup>13</sup>CH<sub>4</sub>; the increase from the documented uncertainties is to represent model transport uncertainty that would otherwise only be resolved by emission changes. The magnitude of model transport will vary between different sites; however, as an estimate here we assume all uncertainties to be equal. By separating the inversion into 12 month intervals the emissions from the previous year are not considered in the inversion for the current year. As a result, December emissions are constrained by fewer observations than January emissions. The influence of this on the posterior error is investigated in section 3.6.

To investigate the effect of including δ<sup>13</sup>CH<sub>4</sub> observations we performed a separate inversion (INV-CH4) using only CH<sub>4</sub> observations. The difference between the inversions indicates the additional information supplied by the inclusion of δ<sup>13</sup>CH<sub>4</sub>. Additional sensitivity experiments were also performed, 9 with varying prior uncertainties and an additional one with no prior trend in annual emissions, to investigate the robustness of the identified trends from the main inversion.

## 2.2 CH<sub>4</sub> and δ<sup>13</sup>CH<sub>4</sub> observations

Monthly mean measurements of CH<sub>4</sub> were taken from 21 National Oceanographic and Atmospheric Administration/Earth System Research Laboratory (NOAA/ESRL) air sampling sites (Dlugokencky *et al.*, 2017) from 2003 to 2015, where available. Measurements of δ<sup>13</sup>CH<sub>4</sub> were taken from 11 NOAA sampling sites and analysed by the Institute of Arctic and Alpine Research (INSTAAR) (White *et al.*, 2017) for the same period (see Table 2). An equal weighting is applied to each monthly mean measurement and potential cross correlations from neighbouring time steps and spatially nearby sites are not considered.

Column-averaged CH<sub>4</sub> (XCH<sub>4</sub>) GOSAT satellite data provided by the University of Leicester were not included in the inversion but retained for independent validation of the inversion results (Parker *et al.*, 2015). GOSAT was omitted because measurements were only available from 2009, 6 years after the inversion began. The Total Carbon Column Observing Network (TCCON) XCH<sub>4</sub> data were ~~also~~ used as validation but were considered too intermittent for use in the inversion (Wunch *et al.*,

2011). Finally, two surface observation sites, The High Altitude Global Climate Observation Center (HAGCOC) in Mexico and Cape Grim in Australia were also used for independent validation.

### 3 Results

#### 3.1 Synthesis Inversion

5 Inversion results constrained by CH<sub>4</sub> and δ<sup>13</sup>CH<sub>4</sub> observations (INV-FULL) show, as expected, improved seasonal and interannual monthly averaged posterior CH<sub>4</sub> and δ<sup>13</sup>CH<sub>4</sub> estimates when compared with assimilated surface observations (Figure 1). The correlation with observations (R) for CH<sub>4</sub> increases from an all-site average of 0.72 in the prior to 0.94 in the posterior, and for δ<sup>13</sup>CH<sub>4</sub> increases from 0.52 to 0.87. Similarly, the root-mean-square error (RMSE) decreases from 38.2 ppb to 9.7 ppb for CH<sub>4</sub> and from 0.25‰ to 0.09‰ for δ<sup>13</sup>CH<sub>4</sub>. The prior model captures some of the initial 2007 CH<sub>4</sub> growth but fails to capture the sustained growth (Figure 1a). The bias in the prior, relative to both the posterior and observations, grows throughout the simulation period. This results in a large bias at the end of the time period, which is evident in the large RMSE values (Figures 1 to 4). The prior also shows a slight decrease in δ<sup>13</sup>CH<sub>4</sub> since 2007, but the magnitude of this is smaller than observed (Figure 1b). The renewed growth of CH<sub>4</sub> and corresponding decrease in δ<sup>13</sup>CH<sub>4</sub> in 2007 are well captured in the inversion.

15 Inversion results constrained by CH<sub>4</sub> (INV-CH4), and not δ<sup>13</sup>CH<sub>4</sub>, also accurately reproduce assimilated CH<sub>4</sub> observations (R = 0.93). INV-CH4 also shows some improved agreement with δ<sup>13</sup>CH<sub>4</sub> observations relative to the prior (R = 0.60), although values are overestimated in earlier years (2003-2008) (Figure 1b).

20 Validation of the model inversion using the independent, non-assimilated GOSAT data shows improved seasonal and interannual representation of XCH<sub>4</sub> (Figure 2). The RMSE is reduced in all 5 regions with values ranging from 48.6 to 64.6 ppb in the prior to 8.3 to 16.5 ppb in the posterior, with values typically originating from a negative bias in the model. The correlation is increased in the inversion with R values ranging from 0.60 to 0.92 in the prior to 0.94 to 0.96 in the posterior. The trend is also better captured in the posterior in all 5 regions, although still underestimated in all regions, more so in EA (-1.3 ppb yr<sup>-1</sup>) and AO (-1.1 ppb yr<sup>-1</sup>). Both the prior and posterior biases are larger in the southern hemisphere, possibly as a result of slow inter-hemispheric transport within the model, previously noted in Patra *et al.* (2011). Also contributing to this offset is an underestimation of southern hemisphere model-simulated atmospheric CH<sub>4</sub> growth rates in the prior model simulation (Figure 3).

30 We performed F further validation is performed using measurements from 9 non-assimilated TCCON sites with data available from at least 2009 (see Table 3). The results show improved model correlation at all 9 sites, with an increase in the all-site mean R value from 0.690-71 in the prior to 0.870-90 in the posterior (Figure 4). Garmisch comparisons are the exception,

where, for unknown reasons, neither the prior nor the posterior accurately captured the observed growth. The RMSE is reduced at 8 out of 9 sites, with an all-site mean decrease from 55.955.3 ppb in the prior to 18.821.4 ppb in the posterior, further reductions would be expected if column observations were used in the inversion. Overall the inversions are found to noticeably improve model performance when validated against the independent measurements from both GOSAT and TCCON. The resulting southern hemisphere offset in the posterior relative to GOSAT and TCCON suggests the posterior estimates represent a reasonable but not conclusive scenario for source/sink attribution. As only surface sites are assimilated, some inaccuracy in the representation of the total column is not surprising, expected.

Two surface sites were omitted from the inversion and retained for independent validation, HAGCOC and Cape Grim. Results show improved model performance in the posterior for both CH<sub>4</sub> and δ<sup>13</sup>CH<sub>4</sub> at Cape Grim and improvement in CH<sub>4</sub> at HAGCOC (Figure 5). There is a slight deterioration in posterior δ<sup>13</sup>CH<sub>4</sub> at HAGCOC relative to the prior. The reasons for this are unclear, however the timeseries of observations at this location are relatively short and only available for later years.

### 3.2 Prior and Posterior Comparison

The synthesis inversions, INV-FULL and INV-CH<sub>4</sub>, provide posterior regional changes in sources and global changes in OH (Figure 6). Relative to the prior, INV-FULL and INV-CH<sub>4</sub> show an average OH decrease of 5% and 4%, respectively (Table 1). Results from INV-FULL show that globally agricultural (-13%), energy (-8%) and biomass burning (+7%) emissions undergo the largest relative average 2003-2015 posterior change compared to the prior (Table 1). Relative changes in rice, waste and wetlands are smaller (<3%). The posterior emission errors are between 5%-13% compared with the 50% prior error. Regionally (Figure 7), 2003-2015 average posterior energy sector emissions are increased, relative to the prior, by 9-33% in four regions (NA, SA, AM and AO), which is offset by a 37% decrease in EA. Notable posterior agricultural emission decreases occur in EA (-36%) and AO (-14%). Wetland emissions are increased beyond the posterior error range in NA (+24%) and EA (+44%) and decreased within the error range in SA (-7%), AM (-7%) and AO (-6%). In all regions posterior emission estimates for biomass burning, waste and rice are within, or close to, the error range compared with prior estimates (Table 4).

Globally, for the 2003-2015 period, derived posterior and prior emission estimates had average growth rates of 4.1±0.6 Tg yr<sup>-2</sup> and 4.0±0.2 Tg yr<sup>-2</sup>, respectively. When considering only the renewed growth (2007-2015) the posterior growth rate of 5.7±0.8 Tg yr<sup>-2</sup> becomes noticeably larger than the prior (3.7±0.4 Tg yr<sup>-2</sup>).

The seasonal range of the prior global wetland emissions (5.7 Tg month<sup>-1</sup>) is underestimated compared to the posterior (13.8 Tg month<sup>-1</sup>). The seasonal cycle in biomass burning emissions is largely unchanged between the prior and posterior. The seasonal amplitude in rice emissions also remains largely unchanged, although the seasonal peak occurs in August in the prior and July in the posterior (Figure 6).

Formatted: Font: Bold

### 3.3 Trends in Sources and Sinks

Formatted: Font: Bold

5 Average energy, waste and wetland emissions are increased post-2007 by  $12.9 \pm 2.7\%$  ( $19.0 \text{ Tg yr}^{-1}$ ),  $5.7 \pm 1.6\%$  ( $3.8 \text{ Tg yr}^{-1}$ ) and  $2.6 \pm 1.8\%$  ( $4.0 \text{ Tg yr}^{-1}$ ), respectively, relative to their 2003-2006 posterior values (Table 6). Regionally, the shift in post-2007 energy sector emissions mainly occurs in AM ( $+8.4 \text{ Tg yr}^{-1}$ ) and AO ( $+11.1 \text{ Tg yr}^{-1}$ ). Four out of five of the regions show a positive post-2007 shift in waste emissions of  $0.4\text{-}1.4 \text{ Tg yr}^{-1}$ , SA is the only region with a slight decrease ( $-0.03 \text{ Tg yr}^{-1}$ ). The small increase in wetland emissions since 2007 derived from the inversion, mainly from EA ( $3.4 \text{ Tg yr}^{-1}$ ), agrees well bottom-up estimates for wetland emission trends, for example the 3% increase found by McNorton *et al.* (2016a). The posterior shows a negative shift in posterior biomass burning emissions  $11.8 \pm 6.4\%$  ( $-2.9 \text{ Tg yr}^{-1}$ ) for the 2007-2015 period relative to 2003-2006, which is in partial agreement with the  $3.7 \text{ Tg CH}_4 \text{ yr}^{-1}$  decrease derived by Worden *et al.* (2017) for the 2008-2014 period relative to 2001-2007. This shift occurs in all five regions, with the largest decrease in AO ( $-1.2 \text{ Tg yr}^{-1}$ ). Overall the derived increase in energy sector, waste and wetland emissions coupled with the decrease in biomass burning emissions agree well with a recent budget review (Saunois *et al.* 2017).

15 The post-2007 posterior emission growth occurs mainly in the energy ( $3.4 \pm 1.0 \text{ Tg yr}^{-2}$ ) and wetland ( $1.4 \pm 1.0 \text{ Tg yr}^{-2}$ ) sectors. For the entire period most of the posterior energy sector growth occurred in AM ( $1.2 \text{ Tg yr}^{-2}$ ) and AO ( $1.5 \text{ Tg yr}^{-2}$ ), with a smaller proportion from NA ( $0.6 \text{ Tg yr}^{-2}$ ) and SA ( $0.2 \text{ Tg yr}^{-2}$ ) (Figure 7 and Table 5). The recent EDGAR v4.3.2 inventory (Janssens-Maenhout *et al.*, 2017) for energy sector emissions shows AM and AO growth of  $1.0 \text{ Tg yr}^{-2}$  and  $2.4 \text{ Tg yr}^{-2}$ , respectively, for 2003-2012. These are, smaller than the  $2.2 \text{ Tg yr}^{-2}$  and  $3.1 \text{ Tg yr}^{-2}$  shown by our inversion for the same period. A majority of prior AM energy sector emissions originate from energy for buildings in Nigeria and Eastern Africa, fuel exploitation from The Middle East, The Niger Delta and South Africa, and pipelines in Western Africa, Algeria and The Middle East. The regional aggregation of fluxes in our inversion system prevents sub-regional attribution, as a result we are unable to diagnose more specific posterior spatial patterns, but our results suggest on a regional scale, emissions are underestimated in both magnitude and growth rate in the prior. For the AO energy sector, a majority of prior emissions, and therefore the posterior increases, originate from energy for buildings in India, China and South-East Asia, fuel exploitation in Eastern China, Japan, India, South East Asia and Eastern Australia, refineries in Northern India, Eastern China, Japan and Indonesia, and pipelines in India Eastern China, Eastern Australia and New Zealand. The growth in emissions in EA in EDGAR v4.3.2 for 2003-2012 ( $1.4 \text{ Tg yr}^{-2}$ ) is not seen in our inversion for the same region and period ( $-2.2 \text{ Tg yr}^{-2}$ ).

30 During the 2008-2012 period NA energy sector emissions were found to be  $11.4 \text{ Tg yr}^{-1}$  (+66%) higher than the 2003-2015 (excluding 2008-2012) average, resulting in uncertainty in the NA growth rate (Figure 6). These findings are also present in INV-CH<sub>4</sub>, which shows an  $11.8 \text{ Tg yr}^{-1}$  increase over the same period. This period of anomalously high emissions is not present in the prior and therefore, is due to the assimilated observations. These high emissions may be associated with oil or natural gas extraction (Helmig *et al.*, 2016). During periods of high NA energy sector emissions, the EA energy sector

emissions are reduced and vis-versa, suggesting a possible dipole caused by the inversion. This suggests increased uncertainty in the derived EA and NA energy sector emissions, possibly due to a paucity of observations over these regions.

5 Posterior wetland emission estimates show a growth of  $0.8 \text{ Tg yr}^{-2}$  for the 2003-2015 period, which increases to  $1.4 \text{ Tg yr}^{-2}$  for the 2007-2015 period. A majority of this growth occurs in EA ( $+0.5 \text{ Tg yr}^{-2}$ ). The four remaining emission sectors all have a global annual change less than  $\pm 0.5 \text{ Tg yr}^{-2}$ .

10 For the posterior time series, OH concentrations in INV-FULL and INV-CH4 are relatively constant throughout the period 2007-2015 (Figure 6) but relative to their 2003-2006 concentrations these values are smaller by  $1.8 \pm 0.4\%$  and  $0.3 \pm 0.5\%$ , respectively. The larger drop post-2007 in INV-FULL OH concentration, relative to INV-CH4, highlights the importance of including  $\delta^{13}\text{CH}_4$  in the inversion. A decrease in OH as a contributor to the renewed growth agrees well with previous simple global box models (Rigby *et al.*, 2017; Turner *et al.*, 2017). The OH shift found here is smaller in magnitude than the -8% shift between 2004 and 2014 derived by Rigby *et al.*, (2017) and the -7% shift between 2003 and 2016 derived by Turner *et al.*, (2017). The posterior OH error is reduced from the prior estimate of 2% to 1.8%, which, although a reduction, is similar to the modelled post-2007 OH decrease. The decrease in OH contributes to a decrease in  $\delta^{13}\text{CH}_4$  and an increase in global  $\text{CH}_4$ . Section 3.5 details analysis of OH sensitivity.

### 3.4 Source and Sink Attribution

20 Analysis performed on our inversion results using the box model approach described by McNorton *et al.* (2016b) suggests that ~30% of the sustained  $\text{CH}_4$  growth post-2007 can be explained by decreased OH, while ~60% and ~10% is attributed to increased energy sector and wetland emissions (Table 5). The shift in emissions between 2003-2006 and 2007-2015 is broadly consistent for each sector for three different inversions, INV\_FULL, INV\_CH4 and INV\_FIXED (fixed annual emissions, see below) (Table 6). We investigated source and sink contribution to the negative  $\delta^{13}\text{CH}_4$  trend using simple one box model analysis, outlined in the appendix of McNorton *et al.* (2016b), and posterior estimates from INV-FULL. Results show that post-2007 changes in energy sector ( $+0.15\%$ ), biomass burning ( $-0.08\%$ ), wetland ( $-0.05\%$ ), waste sector ( $-0.03\%$ ) and agricultural ( $-0.01\%$ ) emissions, as well as OH ( $-0.12\%$ ), contributed to the observed trend.

### 3.2 Source and Sink Attribution

30 The synthesis inversions, INV\_FULL and INV\_CH4, provide posterior regional changes in sources and global changes in OH (Figure 5). Relative to the prior, INV\_FULL and INV\_CH4 show an average OH decrease of 5% and 4%, respectively (Table 1). For the posterior time series, OH concentrations in INV\_FULL and INV\_CH4 are relatively constant throughout the period 2007-2015 (Figure 5) but these values are smaller by  $1.8 \pm 0.4\%$  and  $0.3 \pm 0.5\%$ , respectively, relative to their 2003-2006 concentrations. The larger drop post 2006 in INV\_FULL OH concentration, relative to INV\_CH4, highlights the importance of including  $\delta^{13}\text{CH}_4$  in the inversion. The posterior OH error is reduced from the prior estimate of 2% to 1.8%, which, although

Formatted: Font: Bold

Formatted: Normal

a reduction, is similar to the modelled post-2007 OH decrease. The decrease in OH contributes to a decrease in  $\delta^{13}\text{C}_{\text{CH}_4}$  and an increase in global  $\text{CH}_4$ .

Results from INV-FULL show that globally agricultural (-13%), energy (-8%) and biomass burning (+7%) emissions undergo the largest relative average 2003-2015 posterior change compared to the prior (Table 1). Relative changes in rice, waste and wetlands are smaller ( $<3\%$ ). The posterior emission errors are between 5%–13% compared with the 50% prior error. Average energy and wetland emissions are increased post-2007 by  $12.9 \pm 2.7\%$  ( $19.0 \text{ Tg yr}^{-1}$ ) and  $2.6 \pm 1.8\%$  ( $4.0 \text{ Tg yr}^{-1}$ ), respectively, relative to their 2003-2006 posterior values.

Regionally (Figure 6 and Table 4), 2003-2015 average posterior energy-sector emissions are increased, relative to the prior, by 9-33% in four regions (NA, SA, AM and AO), which is offset by a 37% decrease in EA. Notable posterior agricultural emission decreases occur in EA (-36%) and AO (-14%). Wetland emissions are increased beyond the posterior error range in NA (+24%) and EA (+44%) and decreased within the error range in SA (-7%), AM (-7%) and AO (-6%). In all regions posterior emission estimates for biomass burning, waste and rice are within, or close to, the error range compared with prior estimates.

Our inversion results suggest that ~30% of the sustained  $\text{CH}_4$  growth post-2006 can be explained by decreased OH, while ~60% and ~10% is attributed to increased energy-sector and wetland emissions (Table 5). The shift in emissions between 2003-2006 and 2007-2015 is broadly consistent for each sector for three different inversions, INV-FULL, INV- $\text{CH}_4$  and INV-FIXED (fixed annual emissions, see below) (Table 6). We investigated source and sink contribution to the negative  $\delta^{13}\text{C}_{\text{CH}_4}$  trend using simple one-box model analysis, outlined in the appendix of McNorton *et al.* (2016b), and posterior estimates from INV-FULL. Results show that post-2006 changes in energy sector (+0.15‰), biomass burning (-0.08‰), wetland (-0.05‰), waste sector (-0.03‰) and agricultural (-0.01‰) emissions, as well as OH (-0.12‰), contributed to the observed trend. Globally, for the 2003-2015 period, derived posterior and prior emission estimates had average growth rates of  $4.1 \pm 0.6 \text{ Tg yr}^{-2}$  and  $4.0 \pm 0.2 \text{ Tg yr}^{-2}$ , respectively. When considering only the renewed growth (2007-2015) the posterior growth rate of  $5.7 \pm 0.8 \text{ Tg yr}^{-2}$  becomes noticeably larger than the prior ( $3.7 \pm 0.4 \text{ Tg yr}^{-2}$ ). The post-2007 posterior growth occurs mainly in the energy ( $3.4 \pm 1.0 \text{ Tg yr}^{-2}$ ) and wetland ( $1.4 \pm 1.0 \text{ Tg yr}^{-2}$ ) sectors. For the entire period most of the posterior energy-sector growth occurred in AM ( $1.2 \text{ Tg yr}^{-2}$ ) and AO ( $1.5 \text{ Tg yr}^{-2}$ ), with a smaller proportion from NA ( $0.6 \text{ Tg yr}^{-2}$ ) and SA ( $0.2 \text{ Tg yr}^{-2}$ ) (Figure 6). Posterior wetland emission estimates show a growth of  $0.8 \text{ Tg yr}^{-2}$  for the 2003-2015 period, which increases to  $1.4 \text{ Tg yr}^{-2}$  for the 2007-2015 period. A majority of this growth occurs in EA ( $+0.5 \text{ Tg yr}^{-2}$ ). The four remaining emission sectors all have a global annual change less than  $\pm 0.5 \text{ Tg yr}^{-2}$ .

During the 2008–2012 period NA energy sector emissions were found to be 11.4 Tg yr<sup>-1</sup> (+66%) higher than the 2003–2015 (excluding 2008–2012) average, resulting in uncertainty in the NA growth rate (Figure 5). These findings are also present in INV-CH<sub>4</sub>, which shows an 11.8 Tg yr<sup>-1</sup> increase over the same period. This period of anomalously high emissions is not present in the prior and therefore, is due to the assimilated observations.

The seasonal range of the prior global wetland emissions (5.7 Tg month<sup>-1</sup>) is underestimated compared to the posterior (13.8 Tg month<sup>-1</sup>). The seasonal cycle in biomass burning emissions is largely unchanged between the prior and posterior. The seasonal amplitude in rice emissions also remains largely unchanged, although the seasonal peak occurs in August in the prior and July in the posterior.

Tropospheric Cl only accounts for a small fraction of the total CH<sub>4</sub> sink (~5%) (Kirschke *et al.*, 2013) but, as the KF influence of Cl is more than an order of magnitude greater than that of OH, it is plausible that changes in Cl contribute to the post-2007 trend in δ<sup>13</sup>C-CH<sub>4</sub>. Results from INV-CL (Figure 7) and the sensitivity setup with fixed OH (see Section 3.3) show similar posterior fluxes. This suggests that Cl trends are unlikely to be an important contributor to the post-2007 CH<sub>4</sub> trends, although it is important to note that whilst variability was applied to prior emissions and the OH field, for some years, no variability is applied to the prior Cl field.

### 3.3.5 Sensitivity Tests

To test the robustness of the inversion to changes in prior error estimates we performed nine perturbation experiments (S1–S9). Monthly source errors were perturbed between 10% and 100%, and yearly OH errors from 0% to 10% (Figure 8 and Table 7). For small error perturbations, the inversion results do not change much relative to INV-FULL (Figure 8 and Table 8). However, when the emission errors are reduced from 50% to 10% (S4) the posterior energy emissions estimates deviate from the control (INV-FULL) inversion, with a mean bias of 60.5 Tg yr<sup>-1</sup>. We consider these large ranges in posterior estimates to be an unrealistic representation of interannual variability in energy sector emissions (Figure 8), which suggests the model fails to provide reasonable posterior estimates when the prior emission error is set too low. For most cases of increased emission errors the OH change is similar to the control. However, for 100% emission errors (S6) the agricultural emissions are further reduced, from 82.8 Tg yr<sup>-1</sup> in the prior and 72.1 Tg yr<sup>-1</sup> in INV-FULL, to 64.1 Tg yr<sup>-1</sup>. In this case OH is only reduced by 0.5% post-2006, relative to 2003–2006, compared to 1.8% in INV-FULL. This results in a smaller OH contribution to the post-2006 CH<sub>4</sub> growth.

For a large or small OH errors (S3: 10%, S1: 1%) the posterior OH is decreased by 18% or 2%, respectively, compared to the prior OH. Assuming no change in OH (S9) post-2007 shifts in biomass burning, energy sector and wetland emissions relative to 2003–2006 are required to fit observations in the inversion. In this scenario biomass burning emissions decrease globally by -11.5±3.8% (-2.9 Tg yr<sup>-1</sup>) and in AO by -16.1±17.9% (-1.2 Tg yr<sup>-1</sup>). Energy sector emissions increase globally by 13.6±2.7%

(+20.6 Tg yr<sup>-1</sup>), in NA by 42.9±12.9% (+7.7 Tg yr<sup>-1</sup>) and in AO by 36.7±5.1% (+12 Tg yr<sup>-1</sup>). Wetland emissions increase globally by 3.6±1.8% (+5.8 Tg yr<sup>-1</sup>). The sign and spatial distribution of these changes are similar to those seen in INV-FULL although the magnitude in post-2006<sup>7</sup> changes is typically increased in S9 (see Section 3.2), which is expected as the necessary increased growth rate is allocated more to emission changes when OH is assumed constant.

5

The sensitivity simulations highlight that the prior uncertainty can have a noticeable influence on the posterior estimates. In particular, the posterior OH is found to be sensitive to the prior error estimate, highlighting the importance of prior knowledge for future studies. This limits the accuracy of the magnitude of the posterior estimates. However, the spatial, temporal and sector specific relative post-2007 changes, compared to 2003-2006, remain broadly consistent between experiments. This shows a limitation in the comparison between prior and posterior sources/sinks but does not discount the importance of the results for trend detection between 2003 and 2015.

10

We performed a synthesis inversion with no prior trend in emissions or OH (INV-FIXED), using fixed 2003 emissions, to investigate the sensitivity of the inversion to prescribed prior trend information (Figure-Figure 99). The results show an annual average CH<sub>4</sub> emission growth of 2.8±0.6 Tg yr<sup>-2</sup>, a majority of which comes from the energy sector (1.8±0.6 Tg yr<sup>-2</sup>) and wetlands (0.7±0.5 Tg yr<sup>-2</sup>). On a global scale the sector attribution agrees well with INV-FULL but with a smaller magnitude in emission trends. The reduced growth in INV-FIXED is offset by a higher negative trend in OH concentration (-0.23% yr<sup>-1</sup>), relative to INV\_FULL (-0.14% yr<sup>-1</sup>).

15

20

In absolute terms OH concentrations are 0.8% lower in INV-FIXED compared to INV-FULL, which acts to offset the lower emissions. OH concentrations for INV-FIXED are 1.8% lower for the 2007-2015 period, relative to the 2003-2006 period, matching the relative change from INV-FULL. Regionally, the largest trends are observed over NA (1.2±0.9 Tg yr<sup>-2</sup>), AM (0.9±0.3 Tg yr<sup>-2</sup>) and AO (0.7±0.4 Tg yr<sup>-2</sup>), with over half of the growth in each of those regions originating from the energy sector. Overall INV-FIXED shows good spatial agreement with INV-FULL when considering sector attribution but the magnitude of emission increases is slightly smaller.

25

Tropospheric Cl only accounts for a small fraction of the total CH<sub>4</sub> sink (~5% or less) (Kirschke *et al.*, 2013; Hossaini *et al.*, 2016) but, as the KF influence of Cl is more than an order of magnitude greater than that of OH, it is plausible that changes in Cl contribute to the post-2007 trend in δ<sup>13</sup>CH<sub>4</sub>. Results from an experiment that inverts for CL, INV-CL, (Figure 10) and the sensitivity setup with fixed OH show similar posterior fluxes. This suggests that Cl trends are unlikely to be an important contributor to the post-2007 CH<sub>4</sub> trends, although it is important to note that whilst variability was applied to prior emissions and the OH field, for some years, no variability is applied to the prior Cl field.

30

### 3.6 Posterior Error

The robustness of the experimental setup is further investigated using the posterior error covariance matrix calculated using equation 5. By splitting the inversion into 12 month intervals emissions later in the year are constrained by fewer observations, possibly only by observations close to the source. The influence of this was investigated and the posterior error was found to be on average 12% higher for December emissions relative to the January emissions, which was broadly consistent between regions and sectors.

Relatively small time independent off-diagonal error correlations are found between different regions and sectors (Figure 11). The largest negative correlation is found between EA and NA energy sector emissions, which could explain a potential artefact in the increase in NA emissions over 2008-2012 being offset by a decrease in EA emissions for the same period. Overall the results are well constrained by the inversion. Typically, the temporal error correlation is also found to be relatively small, with the exception being the energy sector emissions. Both positive and negative off-diagonal error correlations are found in posterior energy estimates at a monthly resolution, possibly relating to the prior temporal correlation applied, as a result we typically report annual values.

#### 4 Conclusions

We have performed a synthesis inversion using a 3D3-D CTM to investigate the post-2007 renewed growth in atmospheric CH<sub>4</sub> and decline in  $\delta^{13}\text{CH}_4$ . This work ~~adds to the results from other studies~~ extends on previous work, which ~~were~~ was based on a box-model approach for source and sink attribution based on CH<sub>4</sub> and  $\delta^{13}\text{CH}_4$  observations (e.g. Rigby *et al.*, 2017). By using a 3D3-D CTM we have been able to provide detailed monthly regional attribution of 6 different emission sectors and global OH changes, evaluating both the trends over the full 2003-2015 period and shifts that occurred around 2007. We have also been able to validate these results using independent surface sites and recent XCH<sub>4</sub> data available from GOSAT and TCCON. The sensitivity of the inversion has been tested for different prior assumptions and uncertainties.

A CH<sub>4</sub>-only inversion underconstrains the solution with respect to  $^{13}\text{CH}_4$  observations, resulting in reduced correlation with  $\delta^{13}\text{CH}_4$  observations ( $R = 0.60$ ) larger errors. ~~The constraint improves when the  $\delta^{13}\text{CH}_4$  observations are introduced~~ The agreement of the simulations with observations improved when additional  $^{13}\text{CH}_4$  observations were used to constrain CH<sub>4</sub> fluxes, with the correlation increasing to  $R = 0.87$ . The prior model based on published emissions does not capture the CH<sub>4</sub> and  $\delta^{13}\text{CH}_4$  trend in both the assimilated surface site observations and the non-assimilated GOSAT and TCCON data. In contrast, our derived posterior emission inventories capture both the renewed growth in CH<sub>4</sub> and the reduction in  $\delta^{13}\text{CH}_4$  observed from the assimilated NOAA surface sites from 2007-2015, and compare well with independent surface CH<sub>4</sub> and  $\delta^{13}\text{CH}_4$  observations as well as with GOSAT and TCCON-derived XCH<sub>4</sub>. The independent validation suggests that, although the CH<sub>4</sub> growth rate is better represented in the posterior, it is still underestimated. The posterior model agreement with assimilated surface data and slight bias with validation column data (TCCON and GOSAT) highlights a potential model error

in total column CH<sub>4</sub> concentration; however, this bias is small. The magnitude of the contribution of model transport error to this underestimation is unknown. Both prior and posterior simulations underestimate southern hemisphere CH<sub>4</sub> concentrations, highlighting possible issues with interhemispheric transport within the model. The lack of independent data around the end of the CH<sub>4</sub> 'hiatus' means it is difficult to evaluate model performance over this period (2007).

Our inversion results suggest that the 2007-2015 growth in CH<sub>4</sub> can be best explained by a 1.8±0.4% reduction in mean OH, a 12.9±2.7% increase in energy sector emissions, mainly from AM and AO, and a 2.6±1.8% increase in wetland emissions, mainly from EA. The recent EDGAR v4.3.2 inventory (Janssens-Maenhout *et al.*, 2017) for energy sector emissions shows AM and AO growth of 1.0 Tg yr<sup>-2</sup> and 2.4 Tg yr<sup>-2</sup>, respectively, for 2003-2012. These are, however, smaller than the 2.2 Tg yr<sup>-2</sup> and 3.1 Tg yr<sup>-2</sup> shown by our inversion for the same period. A majority of prior AM energy sector emissions originate from energy for buildings in Nigeria and Eastern Africa, fuel exploitation from The Middle East, The Niger Delta and South Africa, and pipelines in Western Africa, Algeria and The Middle East. As a result emissions from these regions are influenced by posterior emission changes and assumed to be underestimated in both magnitude and growth rate in the prior. For the AO energy sector, a majority of prior emissions, and therefore the posterior increases, originate from energy for buildings in India, China and South East Asia, fuel exploitation in Eastern China, Japan, India, South East Asia and Eastern Australia, refineries in Northern India, Eastern China, Japan and Indonesia, and pipelines in India Eastern China, Eastern Australia and New Zealand. The growth in emissions in EA in EDGAR v4.3.2 (1.4 Tg yr<sup>-2</sup>) is not seen in our inversion for the same region and period (2.2 Tg yr<sup>-2</sup>). We also find higher than average (2005-2015) energy sector emissions over NA between 2008 and 2012, which may be associated with oil or natural gas extraction (Helmig *et al.*, 2016). The expected increase in atmospheric δ<sup>13</sup>CH<sub>4</sub> caused by increased energy sector emissions (+0.15‰) is offset mainly by the decrease in OH (-0.12‰), small decrease in biomass burning emissions (-0.08‰) and small increase in wetland emissions (-0.05‰).

The small increase in wetland emissions since 2007 derived from the inversion agrees well bottom-up estimates for wetland emission trends, for example the 3% increase found by McNorton *et al.* (2016a). A decrease in OH as a contributor to the renewed growth agrees well with previous simple global box models (Rigby *et al.*, 2017; Turner *et al.*, 2017). The OH shift found here is smaller in magnitude than the 8% shift between 2004 and 2014 derived by Rigby *et al.*, (2017) using AGAGE measurements. Our results show a small negative shift in posterior biomass burning emissions (2.9 Tg yr<sup>-1</sup>) for 2007-2015 period relative to 2003-2006, in agreement with the 3.7 Tg CH<sub>4</sub> yr<sup>-1</sup> decrease derived by Worden *et al.* (2017) for the 2008-2014 period relative to 2001-2007.

When δ<sup>13</sup>CH<sub>4</sub> is not assimilated the trend in posterior emissions is slightly increased post-2006 and the OH decrease is smaller (-0.3%). By including the δ<sup>13</sup>CH<sub>4</sub> observations a larger post-2006 OH decrease is required (-1.8%), highlighting the importance of including δ<sup>13</sup>CH<sub>4</sub> within the inversion.

An alternative scenario, where OH is assumed constant post-2007, requires a  $-11.5 \pm 3.8\%$  decrease in biomass burning emissions, and  $13.6 \pm 2.7\%$  and  $3.6 \pm 1.8\%$  increases in energy sector and wetland emissions. These results agree with previous studies, which also assumed constant OH (Nisbet *et al.*, 2016; Schaefer *et al.*, 2016; Worden *et al.*, 2017). Whilst a reduction in OH is found to be, in part, the most likely explanation for the renewed CH<sub>4</sub> growth, this alternative scenario with no change in OH has occurred then this presents provides an alternative explanation for the cause of the post-2007 CH<sub>4</sub> growth.

The inversion results suggest Eurasian energy sector emissions are typically overestimated by inventories and previous top-down studies, such as the Global Carbon Budget (Saunois *et al.*, 2016). The reduced EA emissions are found to be offset by an underestimate in all other regions. We find prior annual estimates of biomass burning, waste and rice to be relatively accurate, whilst agricultural estimates are overestimated. Small changes occur in the seasonal cycle of rice emissions and the seasonal range is underestimated in wetland emissions.

The inversion is found to be robust when small changes are made to uncertainty errors; however, large uncertainty remains around the accuracy of prior emissions. Assuming no prior trend in emissions reduces the required growth rate in both wetland and energy sector emissions, although they remain the main source contribution to the renewed growth post-2007. The reduction in the emission trend is offset by an increased negative trend in OH concentration. Overall the magnitude of the trends inferred varies between experiments but there is consistent agreement that both OH decrease and, wetland and energy sector emission increase contributed to the post-2007 growth.

Our inversion results represent plausible scenarios for variations in CH<sub>4</sub> sources and sinks, though several caveats exist. The uncertainties in the sources and sinks are somewhat subjective and we have not considered source signature and KF uncertainty. We have assumed that all uncertainties are independent of each other (excluding energy emissions). We have also not considered variation in other sinks (e.g. O<sup>1</sup>D, soil). The synthesis inversions are performed over coarse spatial regions and only attribute emissions at the monthly scale, future studies should utilise increased observations to provide finer spatial and temporal resolution. The assumption that emissions within a region are correlated limits more specific spatial attribution of sources. Within a region it is likely that some posterior emissions are too high, offset by emissions being too low elsewhere within the domain. Finally, an important question is whether tropospheric OH has varied in the way suggested by CH<sub>4</sub> inversions studies. The processes causing variations in OH are complex and remain poorly quantified. Possible explanations include changes in tropospheric O<sub>3</sub> and trends in tropospheric UV radiation related to global stratospheric O<sub>3</sub> recovery. If the reduction in available OH due to increased reactive carbon gases is no longer being sufficiently offset by increased emissions of OH-forming nitrogen oxides, then OH concentrations might be in decline (Lelieveld *et al.*, 2004). For example, Itahashi *et al.* (2014) showed a reduction in column NO<sub>2</sub> growth associated with the economic downturn over East Asia between 2008 and 2009, this approximately coincides with the increased CH<sub>4</sub> growth.

## Acknowledgments, Samples, and Data

This work was supported by the NERC MOYA project (NE/N015657/1). MPC and MG acknowledge support from NERC grants GAUGE (NE/K002244/1) and AMAZONICA (NE/F005806/1). RJP was funded via an ESA Living Planet Fellowship with additional funding from the UK National Centre for Earth Observation and the ESA Greenhouse Gas Climate Change Initiative (GHG-CCI). HB was supported by ESA GHG-CCI. CW, RJP and HB acknowledge funding support as part of NERC's National Centre for Earth Observation, contract number PR140015. The TOMCAT runs were performed on the Arc3 supercomputer at U. Leeds. We thank the Japanese Aerospace Exploration Agency, National Institute for Environmental Studies, and the Ministry of Environment for the GOSAT data and their continuous support as part of the Joint Research Agreement. The GOSAT retrievals used the ALICE High Performance Computing Facility at the University of Leicester.

5 NOAA atmospheric CH<sub>4</sub> and δ<sup>13</sup>CH<sub>4</sub> values were obtained from the ESRL GMD Carbon Cycle Cooperative Global Air Sampling Network (esrl.noaa.gov). TCCON atmospheric column CH<sub>4</sub> values were obtained from the TCCON data archive (tccodata.org). The authors would also like to thank Matt Rigby for advice with <sup>13</sup>CH<sub>4</sub> modelling.

All model data used in this study are available through the University of Leeds ftp server. For access please contact

15 M.Chipperfield@leeds.ac.uk.

## References

Bergamaschi, P., Frankenberg, C., Meirink, J.F., Krol, M., Dentener, F., Wagner, T., Platt, U., Kaplan, J.O., Körner, S., Heimann, M. and Dlugokencky, E.J.: Satellite cartography of atmospheric methane from SCIAMACHY on board ENVISAT: 2. Evaluation based on inverse model simulations, *J. Geophys. Res.: Atmos.*, *112*, D02304, doi: 10.1029/2006JD007268, 2007.

20 Blumenstock, T., Hase, F., Schneider, M., García, O.E. and Sepúlveda, E.: TCCON data from Izana, Tenerife, Spain, Release GGG2014R1. TCCON data archive, hosted by CaltechDATA, California Institute of Technology, Pasadena, CA, U.S.A., doi:10.14291/tcon.ggg2014.izana01.R1, 2017.

25 Bousquet, P., Ciais, P., Miller, J.B., Dlugokencky, E.J., Hauglustaine, D.A., Prigent, C., Van der Werf, G.R., Peylin, P., Brunke, E.G., Carouge, C. and Langenfelds, R.L.: Contribution of anthropogenic and natural sources to atmospheric methane variability, *Nature*, *443*, 439-443, doi:10.1038/nature05132, 2006.

30 Bousquet, P., Ringeval, B., Pison, I., Dlugokencky, E.J., Brunke, E.G., Carouge, C., Chevallier, F., Fortems-Cheiney, A., Frankenberg, C., Hauglustaine, D.A. and Krummel, P.B.: Source attribution of the changes in atmospheric methane for 2006–2008, *Atmos. Chem. Phys.*, *11*, 3689-3700, doi:10.5194/acp-11-3689-2011, 2011.

Chipperfield, M.: New version of the TOMCAT/SIMCAT off-line chemical transport model: Intercomparison of stratospheric tracer experiments, *Q. J. Roy. Meteorol. Soc.*, 132, 1179-1203, doi:10.1256/qj.05.51, 2006.

Dee, D.P., Uppala, S.M., Simmons, A.J., Berrisford, P., Poli, P., Kobayashi, S., Andrae, U., Balmaseda, M.A., Balsamo, G.,  
5 Bauer, D.P. and Bechtold, P.: The ERA-Interim reanalysis: Configuration and performance of the data assimilation system, *Q. J. Roy. Meteorol. Soc.*, 137, 553-597, doi:10.1002/qj.828, 2011.

DeFries, R. S. and Townshend, J. R. G.: NDVI-derived land cover classification at a global scale. *Int. J. Remote Sens.*, 15, 3567-3586, doi:10.1080/01431169408954345, 1994.

10 Dlugokencky, E.J., Lang, P.M., Crotwell, A.M., Mund, J.W., Crotwell, M.J. and Thoning, K.W.: Atmospheric Methane Dry Air Mole Fractions from the NOAA ESRL Carbon Cycle Cooperative Global Air Sampling Network, 1983-2016, Version: 2017-07-28, Path: ftp://aftp.cmdl.noaa.gov/data/trace\_gases/ch4/flask/surface/, 2017.

15 Griffith, D. W. T., *et al.*: TCCON data from Darwin, Australia, Release GGG2014R0. TCCON data archive, hosted by CaltechDATA, California Institute of Technology, Pasadena, CA, U.S.A. doi:10.14291/tcon.ggg2014.darwin01.R0/1149290, 2017a.

20 Griffith, D. W. T., Velazco, V. A., Deutscher, N., Murphy, C., Jones, N., Wilson, S., Macatangay, R., Kettlewell, G., Buchholz, R. R., Riggenschbach, M.: TCCON data from Wollongong, Australia, Release GGG2014R0. TCCON data archive, hosted by CaltechDATA, California Institute of Technology, Pasadena, CA, U.S.A. doi:10.14291/tcon.ggg2014.wollongong01.R0/1149291, 2017b.

25 Helmig, D., Rossabi, S., Hueber, J., Tans, P., Montzka, S.A., Masarie, K., Thoning, K., Plass-Duelmer, C., Claude, A., Carpenter, L.J. and Lewis, A.C.: Reversal of global atmospheric ethane and propane trends largely due to US oil and natural gas production, *Nat. Geosci.*, 9, 490-495, doi:10.1038/ngeo2721, 2016.

30 Hossaini, R., Chipperfield, M.P., Saiz-Lopez, A., Fernandez, R., Monks, S., Feng, W., Brauer, P. and Glasow, R.: A global model of tropospheric chlorine chemistry: Organic versus inorganic sources and impact on methane oxidation, *J. Geophys. Res.*, 121, 14271-14297, doi:10.1002/2016JD025756, 2016.

Itahashi, S., Uno, I., Irie, H., Kurokawa, J.-I., and Ohara, T.: Regional modeling of tropospheric NO<sub>2</sub> vertical column density over East Asia during the period 2000–2010: comparison with multisatellite observations. *Atmos. Chem. Phys.*, 14, 3623-3635, https://doi.org/10.5194/acp-14-3623-2014, 2014.

Formatted: Font: Italic

- Janssens-Maenhout, G., Crippa, M., Guizzardi, D., Muntean, M. and Schaaf, E.: Emissions Database for Global Atmospheric Research, version v4.3.2 part I Greenhouse gases (gridmaps). European Commission, Joint Research Centre (JRC) [Dataset]. Available from [https://data.europa.eu/doi/10.2904/JRC\\_DATASET\\_EDGAR](https://data.europa.eu/doi/10.2904/JRC_DATASET_EDGAR) [Accessed 17<sup>th</sup> April 2018], 2017.
- 5 Janssens-Maenhout, G., Crippa, M., Guizzardi, D., Muntean, M., Schaaf, E., Dentener, F., Bergamaschi, P., Pagliari, V., Olivier, J.G.J., Peters, J.A.H.W. and Van Aardenne, J.A.: EDGAR v4.3.2 Global Atlas of the three major Greenhouse Gas Emissions for the period 1970-2012, *Earth Sys. Sci. Data Discuss.*, in review, doi:10.5194/essd-2017-79, 2017.
- Kirschke, S., Bousquet, P., Ciais, P., Saunois, M., Canadell, J.G., Dlugokencky, E.J., Bergamaschi, P., Bergmann, D., Blake,  
10 D.R., Bruhwiler, L. and Cameron-Smith, P.: Three decades of global methane sources and sinks, *Nat. Geosci.*, *6*, 813-823, doi:10.1038/ngeo1955, 2013.
- Kivi, R., Heikkinen, P. and Kyro, E.: TCCON data from Sodankyla, Finland, Release GGG2014R0. TCCON data archive, hosted by CaltechDATA, California Institute of Technology, Pasadena, CA, U.S.A.  
15 doi:10.14291/tcon.ggg2014.sodankyla01.R0/1149280, 2017.
- Lelieveld, J., Dentener, F.J., Peters, W. and Krol, M.C.: On the role of hydroxyl radicals in the self-cleansing capacity of the troposphere, *Atmos. Chem. Phys.*, *4*, 2337-2344, doi:10.5194/acp-4-2337-2004, 2004.
- 20 Liang, Q., Chipperfield, M.P., Fleming, E.L., Abraham, N.L., Braesicke, P., Burkholder, J.B., Daniel, J.S., Dhomse, S., Fraser, P.J., Hardiman, S.C. and Jackman, C.H.: Deriving Global OH Abundance and Atmospheric Lifetimes for Long-Lived Gases: A Search for CH<sub>3</sub>CCl<sub>3</sub> Alternatives, *J. Geophys. Res.: Atmos.*, *122*, 11914-11933, doi:10.1002/2017JD026926, 2017.
- McNorton, J., Gloor, E., Wilson, C., Hayman, G.D., Gedney, N., Comyn-Platt, E., Marthews, T., Parker, R.J., Boesch, H. and  
25 Chipperfield, M.P.: Role of regional wetland emissions in atmospheric methane variability. *Geophys. Res. Lett.*, *43(21)*, L11433, doi:10.1002/2016GL070649, 2016.
- McNorton, J., Chipperfield, M.P., Gloor, M., Wilson, C., Feng, W., Hayman, G.D., Rigby, M., Krummel, P.B., O'Doherty, S., Prinn, R.G. and Weiss, R.F.: Role of OH variability in the stalling of the global atmospheric CH<sub>4</sub> growth rate from 1999 to  
30 2006, *Atmos. Chem. Phys.*, *16*, 7943-7956, doi:10.5194/acp-16-7943-2016, 2016b.
- Montzka, S.A., Krol, M., Dlugokencky, E., Hall, B., Jöckel, P. and Lelieveld, J.: Small interannual variability of global atmospheric hydroxyl, *Science*, *331*, 67-69, doi:10.1126/science.1197640, 2011.

- Nisbet, E.G., Dlugokencky, E.J. and Bousquet, P.: Methane on the rise—again, *Science*, *343*(6170), 493-495, doi:10.1126/science.1247828, 2014.
- Nisbet, E.G., Dlugokencky, E.J., Manning, M.R., Lowry, D., Fisher, R.E., France, J.L., Michel, S.E., Miller, J.B., White, J.W.C., Vaughn, B. and Bousquet, P.: Rising atmospheric methane: 2007–2014 growth and isotopic shift, *Global Biogeochem. Cycles*, *30*(9), 1356-1370, doi:10.1002/2016GB005406, 2016.
- Notholt, J., Schrems, O., Warneke, T., Deutscher, N., Weinzierl, C., Palm, M., Buschmann, M., and AWI-PEV Station Engineers: TCCON data from Ny Alesund, Spitzbergen, Norway, Release GGG2014R0. TCCON data archive, hosted by CaltechDATA, California Institute of Technology, Pasadena, CA, U.S.A. doi:10.14291/tcon.ggg2014.nyalesund01.R0/1149278, 2017a.
- Notholt, J., Petri, C., Warneke, T., Deutscher, N., Buschmann, M., Weinzierl, C., Macatangay, R. and Grupe, P.: TCCON data from Bremen, Germany, Release GGG2014R0. TCCON data archive, hosted by CaltechDATA, California Institute of Technology, Pasadena, CA, U.S.A. doi:10.14291/tcon.ggg2014.bremen01.R0/1149275, 2017b.
- Parker, R., Boesch, H., Byckling, K., Webb, A.J., Palmer, P.I., Feng, L., Bergamaschi, P., Chevallier, F., Notholt, J. and Deutscher N.: Assessing 5 years of GOSAT Proxy XCH<sub>4</sub> data and associated uncertainties, *Atmos. Meas. Tech.*, *8*, 4785-4801, doi:10.5194/amtd-8-5937-2015, 2015.
- Patra, P.K., Houweling, S., Krol, M., Bousquet, P., Belikov, D., Bergmann, D., Bian, H., Cameron-Smith, P., Chipperfield, M.P., Corbin, K. and Fortems-Cheiney, A.: TransCom model simulations of CH<sub>4</sub> and related species: linking transport, surface flux and chemical loss with CH<sub>4</sub> variability in the troposphere and lower stratosphere, *Atmos. Chem. Phys.*, *11*, 12813-12837, doi:10.5194/acp-11-12813-2011, 2011.
- Rice, A.L., Butenhoff, C.L., Teama, D.G., Röger, F.H., Khalil, M.A.K. and Rasmussen, R.A.: Atmospheric methane isotopic record favors fossil sources flat in 1980s and 1990s with recent increase, *Proc. Natl. Acad. Sci.*, *113*(39), 10791-10796, doi:10.1073/pnas.1522923113, 2016.
- Rigby, M., Manning, A.J. and Prinn, R.G.: The value of high-frequency, high-precision methane isotopologue measurements for source and sink estimation, *J. Geophys. Res.*, *117*, D12312, doi:10.1029/2011JD017384, 2012.

Rigby, M., Montzka, S.A., Prinn, R.G., White, J.W., Young, D., O'Doherty, S., Lunt, M.F., Ganesan, A.L., Manning, A.J., Simmonds, P.G. and Salameh, P.K.: Role of atmospheric oxidation in recent methane growth, *Proc. Natl. Acad. Sci.*, *114*(21), 5373-5377, doi:10.1073/pnas.1616426114, 2017.

5 Saunois, M., et al.: The global methane budget 2000–2012, *Earth Syst. Sci. Data*, *8*, 697-751, doi: 10.5194/essd-8-697-2016, 2016.

Saunois, M., et al.: Variability and quasi-decadal changes in the methane budget over the period 2000–2012, *Atmos. Chem. Phys.*, *17*, 11135-11161, <https://doi.org/10.5194/acp-17-11135-2017>, 2017.

Formatted: Font: Italic

Formatted: Font: Italic

10

Schaefer, H., Fletcher, S.E.M., Veidt, C., Lassey, K.R., Brailsford, G.W., Bromley, T.M., Dlugokencky, E.J., Michel, S.E., Miller, J.B., Levin, I. and Lowe, D.C.: A 21st-century shift from fossil-fuel to biogenic methane emissions indicated by <sup>13</sup>CH<sub>4</sub>, *Science*, *352*, 80-84, doi:10.1126/science.aad2705, 2016.

15 Schwietzke, S., Sherwood, O.A., Bruhwiler, L.M., Miller, J.B., Etiopie, G., Dlugokencky, E.J., Michel, S.E., Arling, V.A., Vaughn, B.H., White, J.W. and Tans, P.P.: Upward revision of global fossil fuel methane emissions based on isotope database, *Nature*, *538*(7623), 88-91, doi:10.1038/nature19797, 2016.

20 Sussmann, R. and Rettinger, M.: TCCON data from Garmisch, Germany, Release GGG2014R1. TCCON data archive, hosted by CaltechDATA, California Institute of Technology, Pasadena, CA, U.S.A. <https://doi.org/10.14291/tcon.ggg2014.garmisch01.R1>, 2017.

Turner, A.J., Frankenberg, C., Wennberg, P.O. and Jacob, D.J.: Ambiguity in the causes for decadal trends in atmospheric methane and hydroxyl, *Proc. Natl. Acad. Sci.*, *114*(21), 5367-5372, doi:10.1073/pnas.1616020114, 2017.

25

Wennberg, P. O., Roehl, C., Wunch, D., Toon, G. C., Blavier, J.-F., Washenfelder, R., Keppel-Aleks, G., Allen, N. and Ayers, J.: TCCON data from Park Falls, Wisconsin, USA, Release GGG2014R1. TCCON data archive, hosted by CaltechDATA, California Institute of Technology, Pasadena, CA, U.S.A. doi:10.14291/tcon.ggg2014.parkfalls01.R1, 2017a.

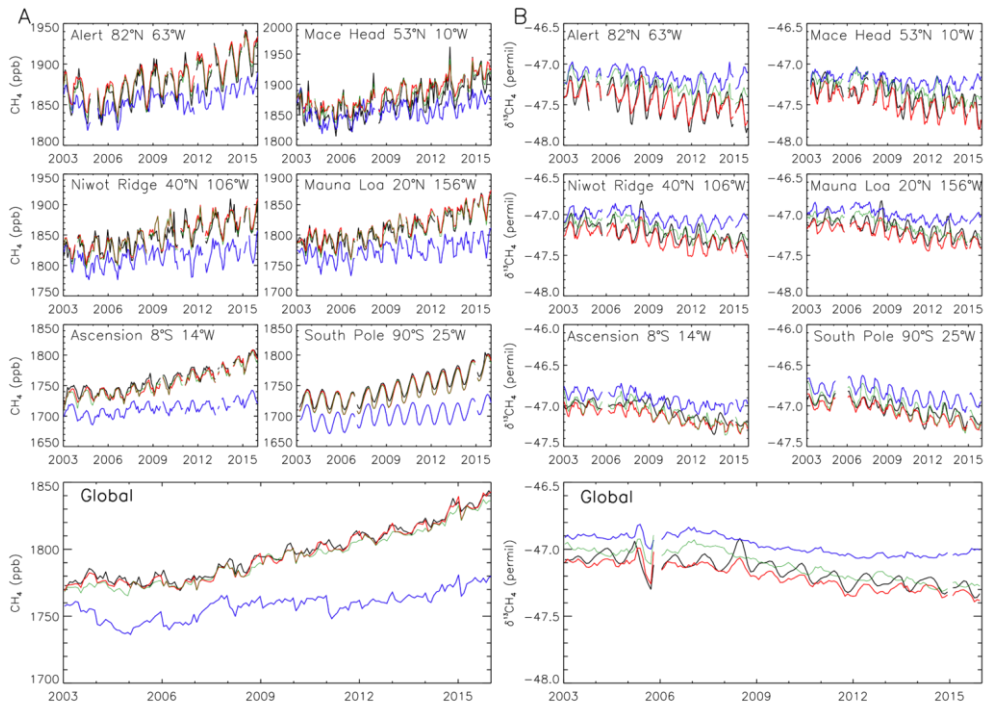
30 Wennberg, P. O., Wunch, D., Roehl, C., Blavier, J.-F., Toon, G. C., Allen, N., Dowell, P., Teske, K., Martin, C. and Martin, J.: TCCON data from Lamont, Oklahoma, USA, Release GGG2014R1. TCCON data archive, hosted by CaltechDATA, California Institute of Technology, Pasadena, CA, U.S.A. doi:10.14291/tcon.ggg2014.lamont01.R1/1255070, 2017b.

White, J.W.C., Vaughn, B.H. and Michel, S.E.: University of Colorado, Institute of Arctic and Alpine Research (INSTAAR), Stable Isotopic Composition of Atmospheric Methane ( $^{13}\text{C}$ ) from the NOAA ESRL Carbon Cycle Cooperative Global Air Sampling Network, 1998-2015, Version: 2017-01-20, Path: [ftp://aftp.cmdl.noaa.gov/data/trace\\_gases/ch4c13/flask/](ftp://aftp.cmdl.noaa.gov/data/trace_gases/ch4c13/flask/), 2017.

- 5 Worden, J.R., Bloom, A.A., Pandey, S., Jiang, Z., Worden, H.M., Walker, T.W., Houweling, S. and Röckmann, T.: Reduced biomass burning emissions reconcile conflicting estimates of the post-2006 atmospheric methane budget, *Nat. Commun.*, *8*(1), 2227, doi:10.1038/s41467-017-02246-0, 2017.

- Wilson, C., Gloor, M., Gatti, L.V., Miller, J.B., Monks, S.A., McNorton, J., Bloom, A.A., Basso, L.S. and Chipperfield, M.P.:  
10 Contribution of regional sources to atmospheric methane over the Amazon Basin in 2010 and 2011, *Global Biogeochem. Cycles*, *30*(3), 400-420, doi:10.1002/2015GB005300, 2016.

- Wunch, D., Toon, G.C., Blavier, J.F.L., Washenfelder, R.A., Notholt, J., Connor, B.J., Griffith, D.W., Sherlock, V. and  
15 Wennberg, P.O.: The total carbon column observing network, *Philos. Trans. Royal Soc. A.*, *369*(1943), 2087-2112, doi:10.098/rsta.2010.0240, 2011



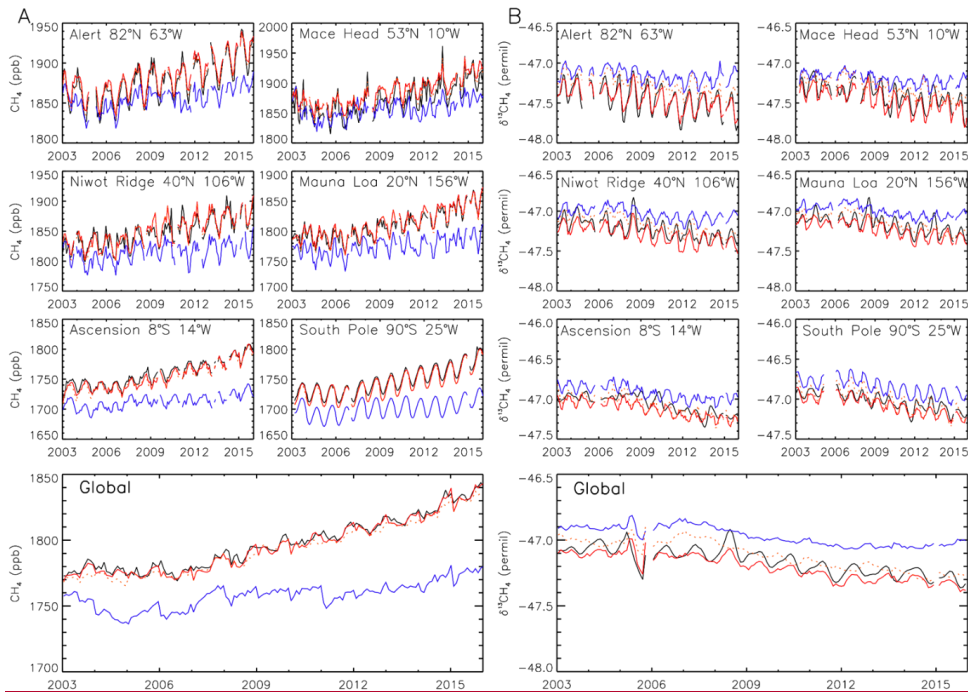


Figure 1. (a) Observed surface  $\text{CH}_4$  (ppb, black solid-line) from 2003 to 2015 at 6 selected NOAA sites and global mean. Also shown are results from TOMCAT simulations using prior emission estimates (blue line), posterior estimates based on a  $\text{CH}_4$  synthesis inversion (INV- $\text{CH}_4$ , green line) and posterior estimates based on a combined  $\text{CH}_4$  and  $\delta^{13}\text{CH}_4$  synthesis inversion (INV-FULL, red line). (b) Same as (a) but for observed and modelled  $\delta^{13}\text{CH}_4$ . Global averages are based on site interpolations onto  $180\ 1^\circ$ -latitude bins, which are weighted by surface area.

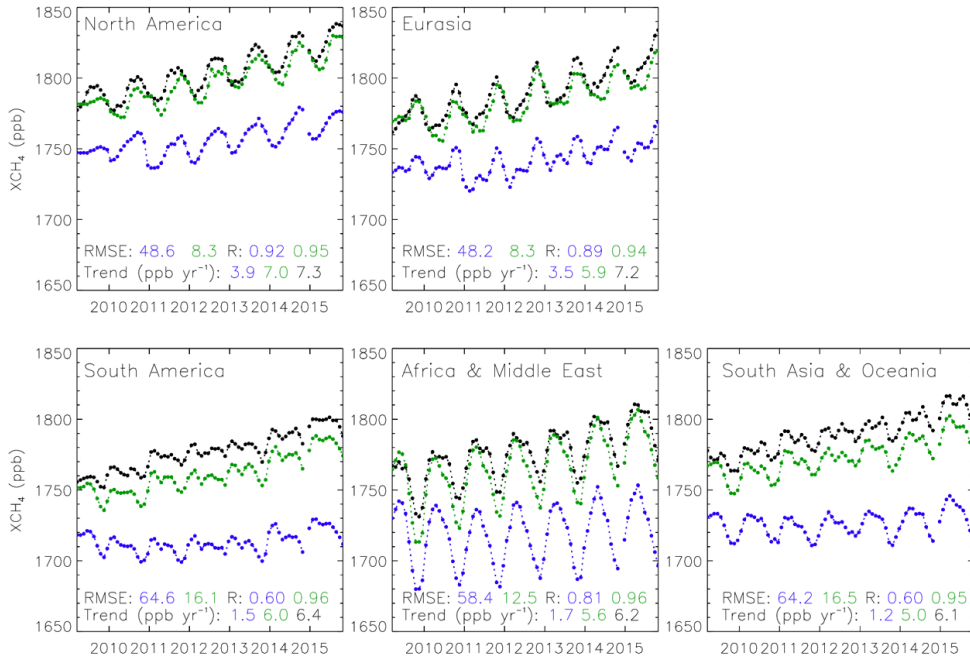
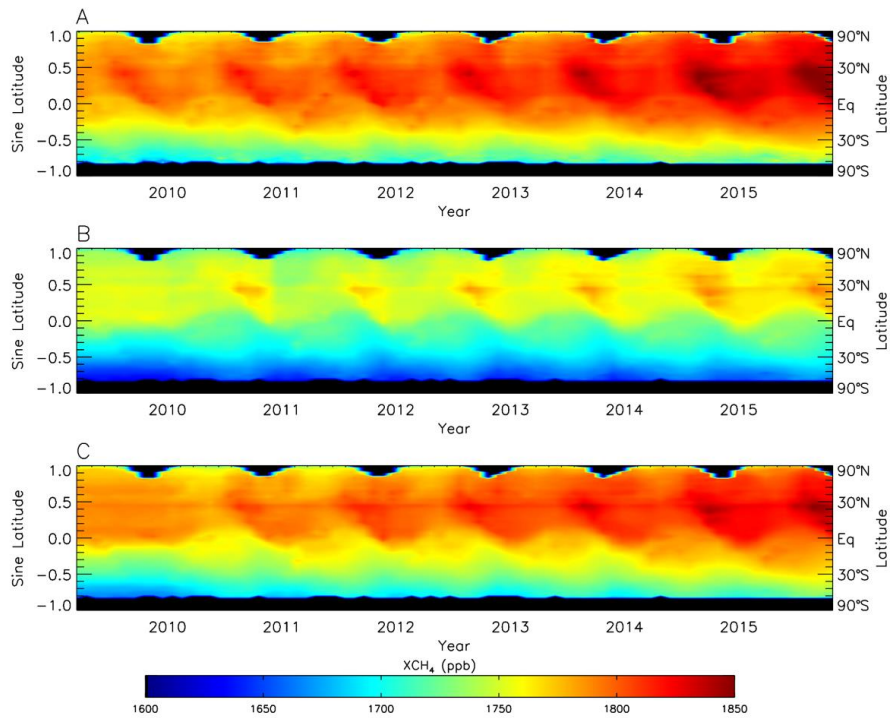
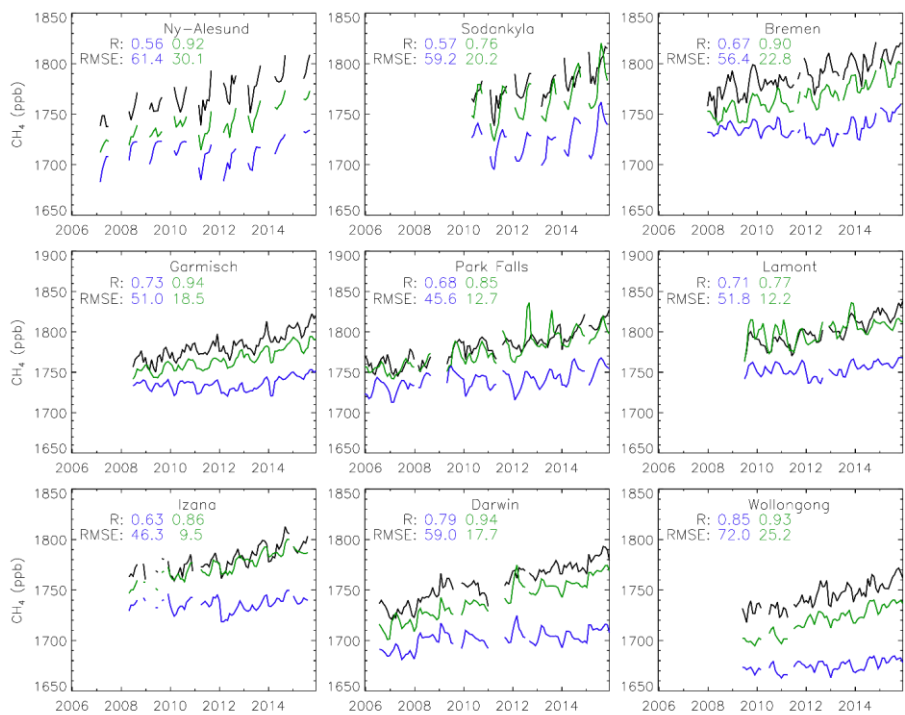


Figure 2. Monthly mean XCH<sub>4</sub> volume mixing ratio (ppb) from GOSAT between April 2009 and December 2015 (black line) for 5 emission regions. Also shown are results from TOMCAT simulations with prior (blue) and posterior (green) emission estimates, both with GOSAT averaging kernels applied. Correlation coefficients, RMSE and growth rates of the model simulations and GOSAT in each region are shown in the panels.

5



**Figure 3.** (a) Zonally averaged monthly mean XCH<sub>4</sub> volume mixing ratio (ppb) from GOSAT between April 2009 and December 2015 plotted against the sine of latitude, where black denotes missing values. (b and c) Same as (a) but for TOMCAT simulations with prior and posterior emission estimates, respectively. GOSAT averaging kernels are applied to model simulations.



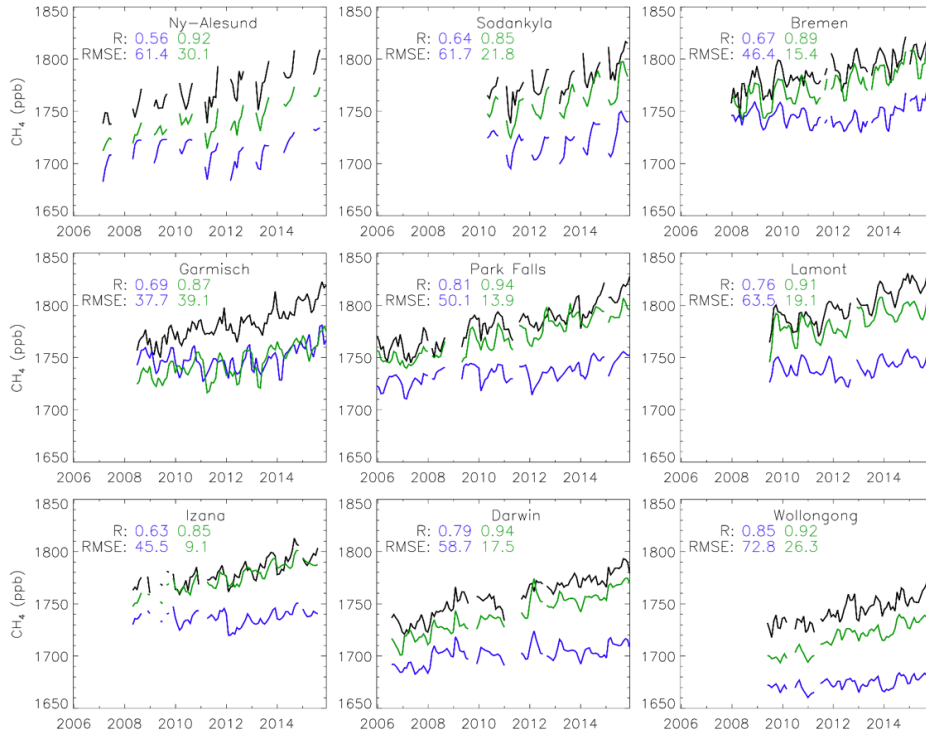


**Figure 4. Observed monthly mean XCH<sub>4</sub> volume mixing ratio (ppb) (blackline) at 9 TCCON sites. Also shown are results from TOMCAT simulations with prior (blue) and posterior (green) emission estimates, both with TCCON averaging kernels applied. Correlation coefficients and RMSE of the model simulations compared with TCCON are shown for each site.**

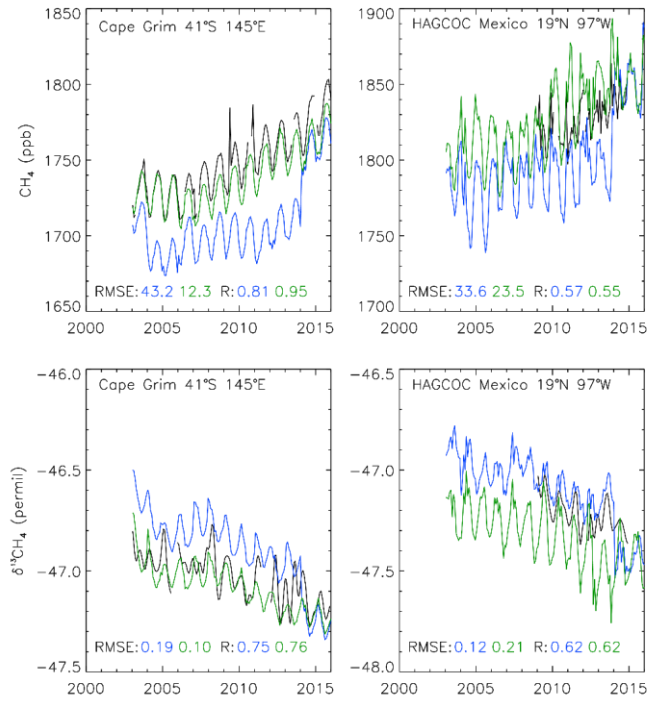


**Figure 5. Observed surface CH<sub>4</sub> (top) and δ<sup>13</sup>CH<sub>4</sub> (bottom) from 2003 to 2015 at 2 independent NOAA sites (black line). Also shown are results from TOMCAT simulations using prior emission estimates (blue line), and posterior estimates based on a combined CH<sub>4</sub> and δ<sup>13</sup>CH<sub>4</sub> synthesis inversion (INV-FULL, green line). RMSE and correlation coefficients of the model simulations compared with observations are shown for each site.**

Formatted: Normal, Centered

Formatted: Font: 9 pt, Bold

Formatted: Normal

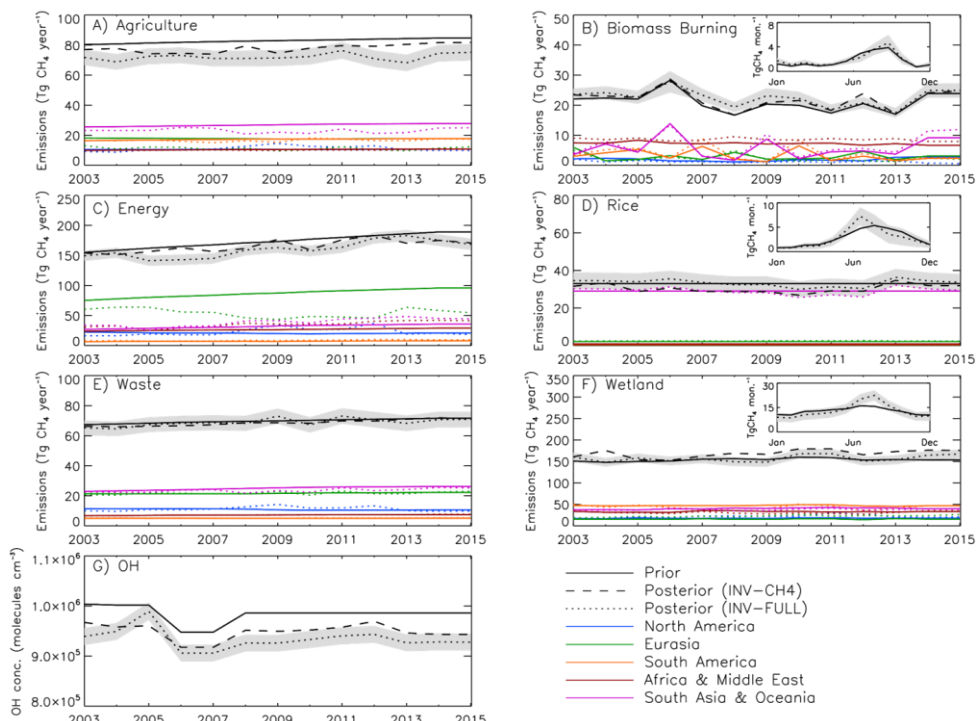


**Figure 6.** (a-f) Annual CH<sub>4</sub> emissions (Tg CH<sub>4</sub> year<sup>-1</sup>) from different sectors for global prior (black solid line), INV-CH<sub>4</sub> (black dashed line) and INV-FULL posterior (black dotted line) estimates. Regional estimates are also displayed for North America (blue), Eurasia (green), South America (orange), Africa and Middle East (red) and South Asia and Oceania (purple). (g) Prior and posterior global OH estimates for the same period. Shaded region denotes posterior error  $A$  for INV-FULL (see Eq. (5) in text).

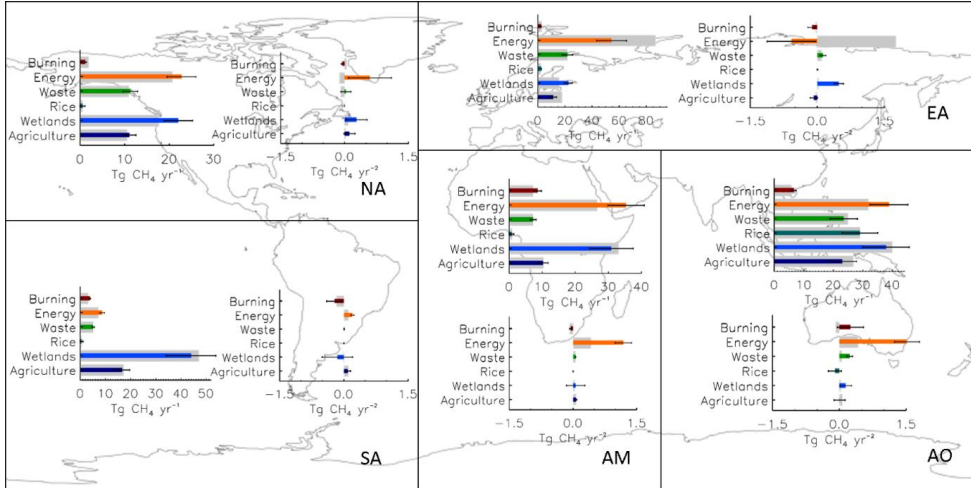
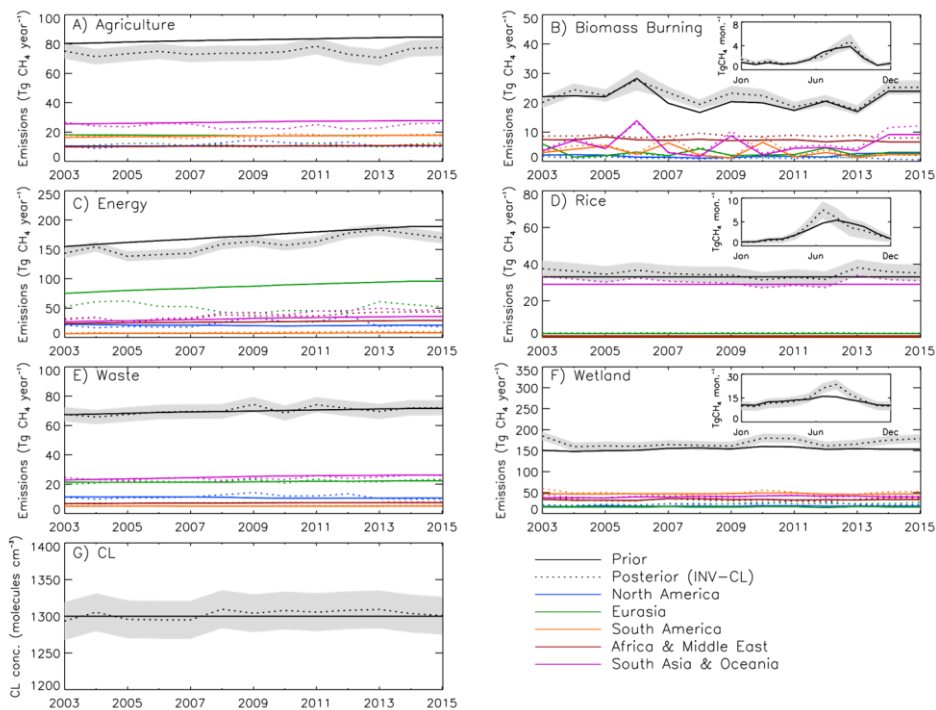


**Figure 6** **Figure 7.** Map showing regional annual mean CH<sub>4</sub> emissions (Tg CH<sub>4</sub> year<sup>-1</sup>) and yearly change in emissions (Tg CH<sub>4</sub> year<sup>-2</sup>) calculated as a linear regression between 2003 and 2015 for INV-FULL (thin coloured bars) and prior (thick grey bars) estimates. Error bars represent one standard deviation of the mean posterior emissions and posterior regression errors. Note that the black borders indicate the 5 regions used for the flux partitioning.



5 **Figure 7.** (a-f) Annual CH<sub>4</sub> emissions (Tg CH<sub>4</sub> year<sup>-1</sup>) from different sectors for global prior (black solid line) and INV-CL (black dotted line) estimates. Regional estimates are also displayed for North America (blue), Eurasia (green), South America (orange), Africa and Middle East (red) and South Asia and Oceania (purple). (g) Prior and posterior global tropospheric CL estimates for the same period. Shaded region denotes posterior error A (see Eq. (5) in text).

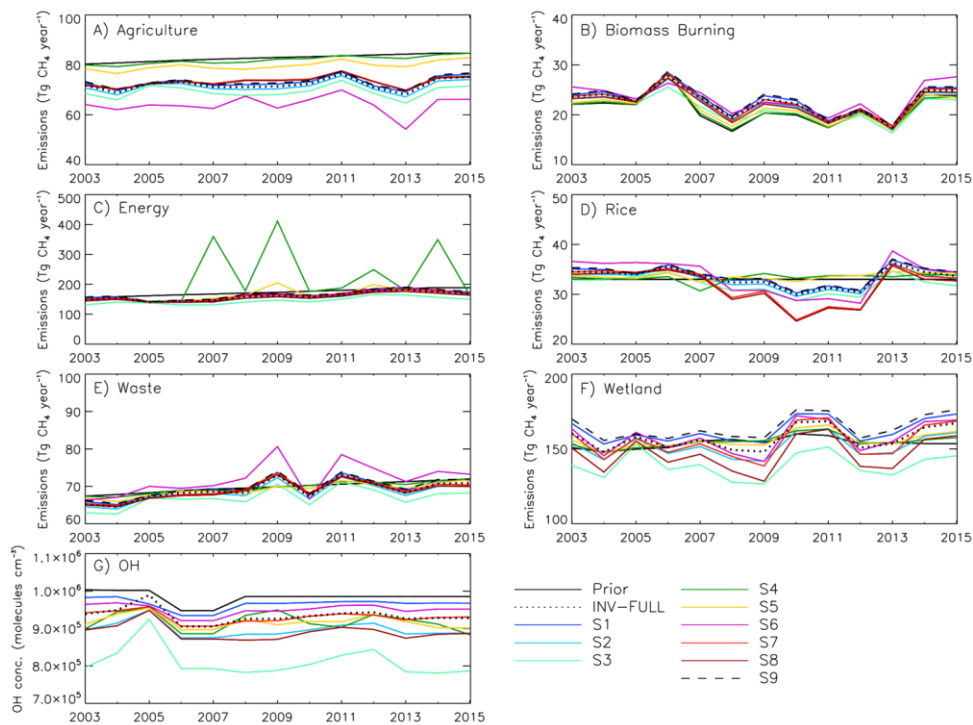


**Figure 8** Figure 8. (a-f) Annual mean CH<sub>4</sub> emissions (Tg CH<sub>4</sub> year<sup>-1</sup>) from different sectors for global prior (black solid line) and INV-FULL (black dotted line) estimates. (g) Same as (a-f) but for global mean OH (molecules cm<sup>-3</sup>). Additional lines in each panel show sensitivity inversions with different emission and OH uncertainties (coloured lines), and an inversion assuming no change in OH (black dashed line).

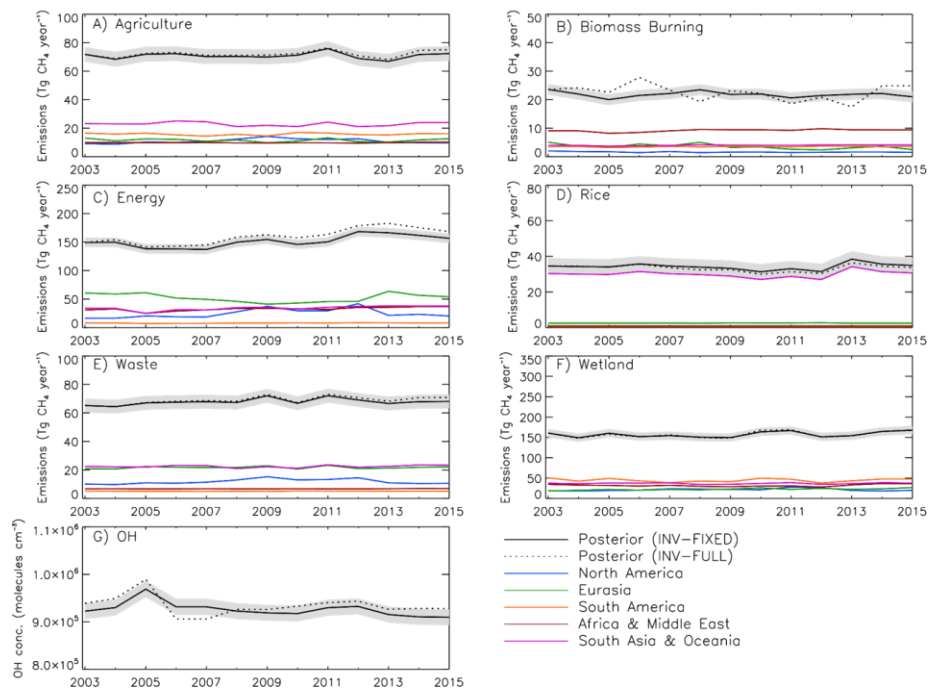


**Figure 9** (a-f) Annual CH<sub>4</sub> emissions (Tg CH<sub>4</sub> year<sup>-1</sup>) from different sectors for INV-FIXED (black solid line) and INV-FULL posterior (black dotted line) estimates. Regional estimates are also displayed for North America (blue), Eurasia (green), South America (orange), Africa and Middle East (red) and South Asia and Oceania (purple). (g) Prior and posterior global OH estimates (molecules cm<sup>-3</sup>) for the same period. Shaded region denotes posterior error A (see Eq. (5) in text).

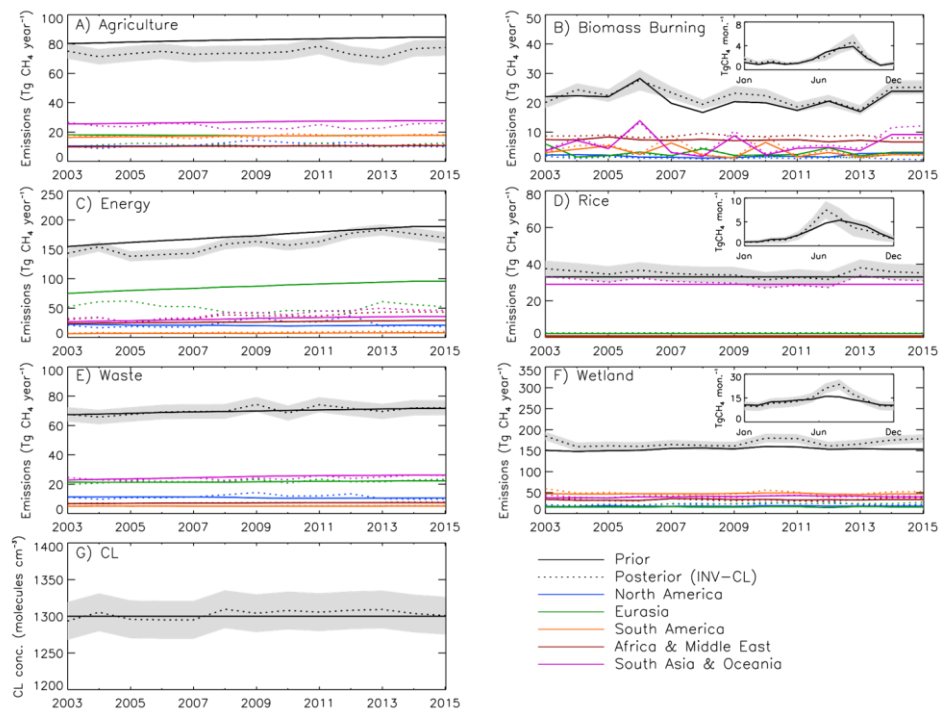


**Figure 10.** (a-f) Annual  $\text{CH}_4$  emissions ( $\text{Tg CH}_4 \text{ year}^{-1}$ ) from different sectors for global prior (black solid line) and INV-CL (black dotted line) estimates. Regional estimates are also displayed for North America (blue), Eurasia (green), South America (orange), Africa and Middle East (red) and South Asia and Oceania (purple). (g) Prior and posterior global tropospheric  $\text{CH}_4$  estimates for the same period. Shaded region denotes posterior error A (see Eq. (5) in text).

5

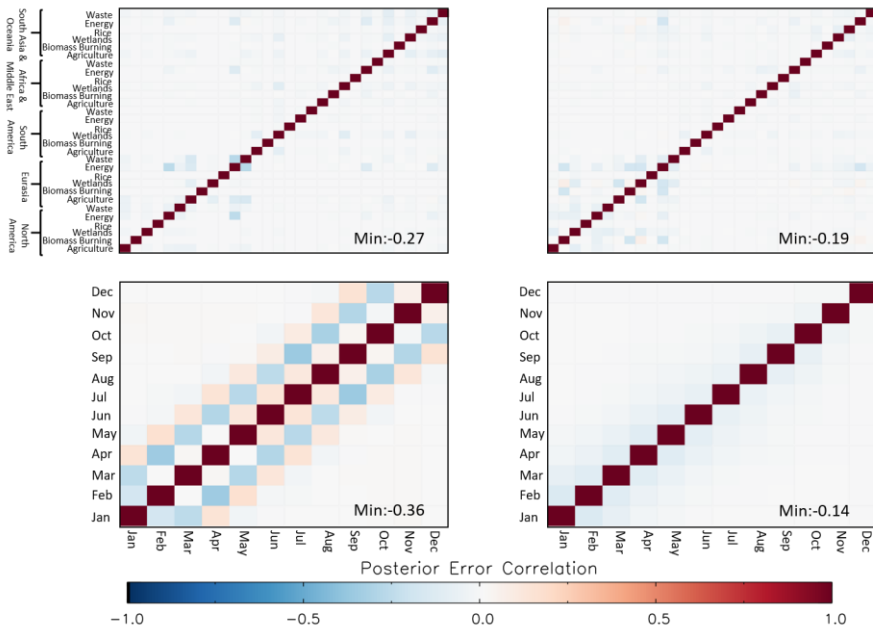


**Figure 11. Posterior error correlation matrix for all regions and sectors for January (top-left) and July (top-right) 2015. Posterior error correlation matrix for 12 months of 2015 for the Eurasian energy sector (bottom-left) and South American wetlands (bottom-right). The plots representshow a subset of the total posterior error correlation matrix as an example.**

**Formatted:** Font: 9 pt, Bold

**Formatted:** Font: 9 pt

**Formatted:** Font: 10 pt, Bold

**Formatted:** Left, Line spacing: single

Source	<u>Interannual variability</u>	$\delta^{13}\text{CH}_4$ (‰)	Emissions for 2003-2015 ( $\text{Tg CH}_4 \text{ yr}^{-1}$ )	
			Prior	Posterior
Agriculture (excluding rice)	<u>Yes</u>	-61.3	82.8	72.1 $\pm$ 5.4
Biomass Burning	<u>Yes</u>	-22.2	21.1	22.5 $\pm$ 2.2
Energy	<u>Yes</u>	-42.6	173.5	160.1 $\pm$ 8.9
Rice	<u>No</u>	-62.0	33.0	33.3 $\pm$ 4.4
Waste	<u>Yes</u>	-55.6	69.8	68.9 $\pm$ 5.1
Wetlands	<u>Yes</u>	-61.0	153.8	157.2 $\pm$ 10.2
Soil	<u>No</u>	22.0	<u>-27.2</u>	-
Methantrophy (negative emission)				
Sink		Kinetic isotope effect ( $^{12}\text{CH}_4/^{13}\text{CH}_4$ )	Average concentration for 2003-2015 (molecules $\text{cm}^{-3}$ )	
			Prior	Posterior
<b>OH</b>	<u>Yes (2003-2007)</u>	1.0039	$0.98 \times 10^6$	$0.93 \times 10^6$
<b>Cl</b>	<u>No</u>	1.06	$1.3 \times 10^3$	$1.3 \times 10^3$
<b>O(<math>^{18}\text{O}</math>)</b>	<u>No</u>	1.013	-	-

Table 1. Source and sink isotope signatures used in the TOMCAT 3-D3-D CTM. Values for prior emissions (Kirschke *et al.*, 2013; McNorton *et al.*, 2016a; Schwietzke *et al.*, 2016) and isotope signatures (Saueressig *et al.*, 2001; Mikaloff-Fletcher *et al.*, 2004; Feilberg *et al.*, 2005; Whiticar *et al.*, 2007; Schwietzke *et al.*, 2016) are based on previous studies. Note that the soil sink is not optimised and modelled as a negative emission. Posterior emission estimates are shown with posterior error estimates.

Formatted Table

Site Code	Site Name	Latitude (°N)	Longitude (°E)	Altitude (m)	Measurements
ALT	Alert, Canada	82.5	-62.5	190.0	CH <sub>4</sub> , δ <sup>13</sup> CH <sub>4</sub>
ASC	Ascension Island, UK	-8.0	-14.4	85.0	CH <sub>4</sub> , δ <sup>13</sup> CH <sub>4</sub>
AZR	Terceira Island, Portugal	38.8	-27.4	19.0	CH <sub>4</sub> , δ <sup>13</sup> CH <sub>4</sub>
BRW	Barrow, USA	71.3	-156.6	11.0	CH <sub>4</sub> , δ <sup>13</sup> CH <sub>4</sub>
CBA	Cold Bay, USA	55.2	-162.7	21.3	CH <sub>4</sub>
HBA	Halley Station, UK	-75.6	-26.2	30.0	CH <sub>4</sub>
ICE	Storhofdi, Iceland	63.4	-20.3	118.0	CH <sub>4</sub>
KUM	Cape Kumukahi, USA	19.5	-154.8	3.0	CH <sub>4</sub> , δ <sup>13</sup> CH <sub>4</sub>
MHD	Mace Head, Ireland	53.3	-9.9	5.0	CH <sub>4</sub> , δ <sup>13</sup> CH <sub>4</sub>
MLO	Mauna Loa, USA	19.5	-155.6	3397.0	CH <sub>4</sub> , δ <sup>13</sup> CH <sub>4</sub>
NWR	Niwot Ridge, USA	40.1	-105.6	3523.0	CH <sub>4</sub> , δ <sup>13</sup> CH <sub>4</sub>
PAL	Pallas-Sammaltunturi, Finland	68.0	24.1	565.0	CH <sub>4</sub>
PSA	Palmer Station, USA	-64.9	-64.0	10.0	CH <sub>4</sub>
RPB	Ragged Point, Barbados	13.2	-59.4	15.0	CH <sub>4</sub>
SMO	Tutuila, American Samoa	-14.2	-170.6	42.0	CH <sub>4</sub> , δ <sup>13</sup> CH <sub>4</sub>
SPO	South Pole, USA	-90.0	-24.8	2810.0	CH <sub>4</sub> , δ <sup>13</sup> CH <sub>4</sub>
STM	Ocean Station M, Norway	66.0	2.0	0.0	CH <sub>4</sub>
SUM	Summit, Greenland	72.6	-38.4	3209.5	CH <sub>4</sub>
THD	Trinidad Head, USA	41.1	-124.2	107.0	CH <sub>4</sub>
WLG	Mt. Waliguan, China	36.3	100.9	3810.0	CH <sub>4</sub> , δ <sup>13</sup> CH <sub>4</sub>
ZEP	Ny-Alesund, Norway/Sweden	78.9	11.9	474.0	CH <sub>4</sub>

Table 2. NOAA measurements from 2003 to 2015 used in the synthesis inversions of CH<sub>4</sub> (Dlugokencky *et al.*, 2017) and δ<sup>13</sup>CH<sub>4</sub> (White *et al.*, 2017).

<b>Site Name</b>	<b>Latitude (°N)</b>	<b>Longitude (°E)</b>	<b>Altitude (km)</b>	<b>Reference</b>
Ny-Alesund, Norway	78.9	11.9	0.02	Notholt <i>et al.</i> 2017a
Sodankyla, Finland	67.4	26.6	0.19	Kivi <i>et al.</i> 2017
Bremen, Germany	53.1	8.9	0.03	Notholt <i>et al.</i> 2017b
Garmisch, Germany	47.5	11.1	0.74	Sussmann <i>et al.</i> 2017
Park Falls, USA	45.9	-90.3	0.44	Wennberg <i>et al.</i> 2017a
Lamont, USA	36.6	-97.5	0.32	Wennberg <i>et al.</i> 2017b
Izana, Spain	28.3	-16.5	2.37	Blumenstock <i>et al.</i> 2017
Darwin, Australia	-12.5	130.9	0.04	Griffith <i>et al.</i> 2017a
Wollongong, Australia	-34.4	150.9	0.03	Griffith <i>et al.</i> 2017b

**Table 3.** TCCON sites (Wunch *et al.* 2011) used for evaluation of the TOMCAT simulations.

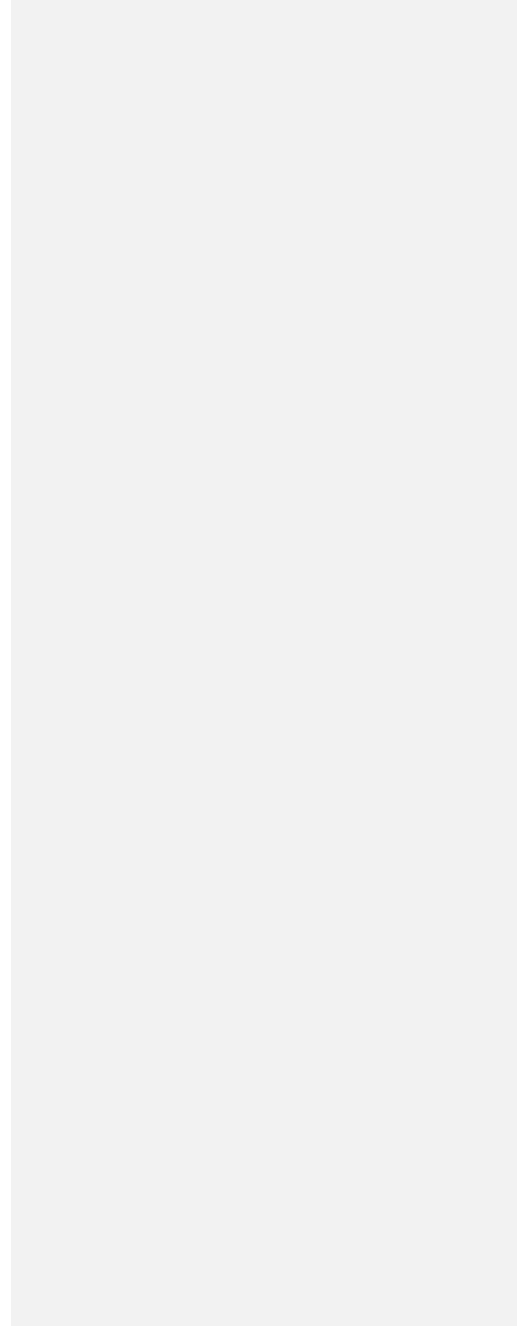
Region	<u>Prior</u> Annual Emissions by Sector (Tg CH <sub>4</sub> year <sup>-1</sup> )						
	<u>Biomass Burning</u>	<u>Energy</u>	<u>Waste</u>	<u>Rice</u>	<u>Wetlands</u>	<u>Agriculture</u>	<u>Total</u>
North America	<u>4.21.9</u>	<u>20.722.8</u>	<u>10.944.2</u>	<u>0.50.5</u>	<u>17.722.0</u>	<u>10.644.0</u>	<u>71.368.7</u>
Eurasia	<u>2.92.3</u>	<u>87.054.4</u>	<u>21.724.7</u>	<u>2.12.5</u>	<u>15.622.5</u>	<u>17.844.2</u>	<u>165.944.6</u>
South America	<u>3.23.8</u>	<u>7.28.7</u>	<u>5.15.4</u>	<u>0.50.5</u>	<u>47.244.0</u>	<u>17.246.6</u>	<u>82.378.7</u>
Africa & Middle East	<u>7.28.6</u>	<u>26.635.4</u>	<u>7.27.2</u>	<u>0.80.8</u>	<u>33.230.8</u>	<u>10.440.2</u>	<u>85.493.4</u>
South Asia & Oceania	<u>5.86.6</u>	<u>32.038.9</u>	<u>24.923.6</u>	<u>29.029.0</u>	<u>40.137.9</u>	<u>26.823.4</u>	<u>177.8459.4</u>
Global	<u>22.521.1</u>	<u>173.5460.4</u>	<u>69.868.9</u>	<u>33.033.3</u>	<u>153.8457.2</u>	<u>82.872.4</u>	<u>594.9537.5</u>

Formatted Table

Region	<u>Posterior</u> Annual Emissions by Sector (Tg CH <sub>4</sub> year <sup>-1</sup> )						
	<u>Biomass Burning</u>	<u>Energy</u>	<u>Waste</u>	<u>Rice</u>	<u>Wetlands</u>	<u>Agriculture</u>	<u>Total</u>
North America	<u>1.2±0.6</u>	<u>22.8±4.0</u>	<u>11.2±2.4</u>	<u>0.5±0.1</u>	<u>22.0±4.0</u>	<u>11.0±2.2</u>	<u>68.7±7.3</u>
Eurasia	<u>2.3±1.0</u>	<u>54.4±11.8</u>	<u>21.7±4.8</u>	<u>2.5±0.6</u>	<u>22.5±3.7</u>	<u>11.2±3.1</u>	<u>114.6±13.9</u>
South America	<u>3.8±1.1</u>	<u>8.7±1.7</u>	<u>5.1±1.2</u>	<u>0.5±0.1</u>	<u>44.0±10.6</u>	<u>16.6±3.8</u>	<u>78.7±15.1</u>
Africa & Middle East	<u>8.6±1.9</u>	<u>35.4±6.3</u>	<u>7.2±1.6</u>	<u>0.8±0.2</u>	<u>30.8±7.4</u>	<u>10.2±2.3</u>	<u>93.1±12.5</u>
South Asia & Oceania	<u>6.6±1.6</u>	<u>38.9±7.2</u>	<u>23.6±5.4</u>	<u>29.0±6.7</u>	<u>37.9±8.6</u>	<u>23.1±5.6</u>	<u>159.1±16.7</u>
Global	<u>22.5±2.9</u>	<u>160.1±15.8</u>	<u>68.9±7.8</u>	<u>33.3±6.8</u>	<u>157.2±16.5</u>	<u>72.1±8.1</u>	<u>537.5±26.5</u>

Table 4. Regional CH<sub>4</sub> emissions based on prior (top) and synthesis inversion estimates (bottom) between 2003 and 2015. Note the total global emission, but not the total regional emissions, include the supplementary emissions (geological, hydrates, oceans and termites). Uncertainties are also shown for posterior emissions, all prior emissions have a 50% uncertainty.

|



Region	Annual Emission Growth by Sector (Tg CH <sub>4</sub> year <sup>-2</sup> )						
	Biomass Burning	Energy	Waste	Rice	Wetlands	Agriculture	Total
North America	-0.06	+0.59	+0.03	+0.00	+0.28	+0.11	+0.95
Eurasia	-0.12	-0.58	+0.13	+0.00	+0.48	-0.08	-0.17
South America	-0.22	+0.20	+0.01	+0.00	-0.15	+0.09	-0.06
Africa & Middle East	-0.05	+1.18	+0.06	+0.00	+0.06	+0.07	+1.33
South Asia & Oceania	+0.25	+1.51	+0.23	-0.10	+0.14	+0.00	+2.03
Global	-0.20	+2.91	+0.46	-0.10	+0.81	+0.20	+4.08

Table 5. Regional CH<sub>4</sub> emission growth trends based on synthesis inversion estimates between 2003 and 2015.

Simulation	Annual Emission by Sector for the 2003-2006 Period (Tg CH <sub>4</sub> year <sup>-1</sup> )						
	Biomass Burning	Energy	Waste	Rice	Wetlands	Agriculture	Total
INV_FULL	24.5	146.9	66.3	34.6	154.4	71.6	518.9
INV_CH4	24.4	156.0	66.3	31.1	160.7	75.9	529.8
INV_FIXED	21.8	143.8	66.1	34.6	155.4	71.1	514.6
	Annual Emission by Sector for the 2007-2015 Period (Tg CH <sub>4</sub> year <sup>-1</sup> )						
	Biomass Burning	Energy	Waste	Rice	Wetlands	Agriculture	Total
INV_FULL	21.6	165.9	70.1	32.7	158.4	72.3	545.8
INV_CH4	20.9	169.9	69.6	30.0	171.9	78.7	557.7
INV_FIXED	21.8	154.5	68.7	34.0	158.1	70.9	536.1
	Difference in Annual Emission Between 2007-2015 and 2003-2006 (Tg CH <sub>4</sub> year <sup>-1</sup> )						
	Biomass Burning	Energy	Waste	Rice	Wetlands	Agriculture	Total
INV_FULL	-2.9	+19.0	+3.8	-1.9	+4.0	+0.7	+26.9
INV_CH4	-3.5	+13.9	+3.3	-1.1	+11.2	+2.8	+27.9
INV_FIXED	0.0	+10.7	+2.6	-0.6	+2.7	-0.2	+21.5

Table 6. Posterior annual CH<sub>4</sub> emission for the period of near-zero atmospheric growth (2003-2006) and the renewed growth (2007-2015) based on three different inversion simulations. Note the total emissions, include the supplementary emissions (geological, hydrates, oceans and termites).

Source/sink	Sensitivity Test Error									
	Control	S1	S2	S3	S4	S5	S6	S7	S8	S9
<b>Wetlands</b>	50%	50%	50%	50%	10%	20%	100%	100%	100%	50%
<b>Rice</b>	50%	50%	50%	50%	10%	20%	100%	100%	100%	50%
<b>Agriculture (excluding rice)</b>	50%	50%	50%	50%	10%	20%	100%	50%	50%	50%
<b>Waste</b>	50%	50%	50%	50%	10%	20%	100%	50%	50%	50%
<b>Energy</b>	50%	50%	50%	50%	10%	20%	100%	50%	50%	50%
<b>Biomass Burning</b>	50%	50%	50%	50%	10%	20%	100%	50%	50%	50%
<b>OH</b>	2%	1%	3%	10%	2%	2%	2%	2%	3%	0%

Table 7. Suite of inversion sensitivity experiments with varying errors on source and sink estimates.

